CHALMERS

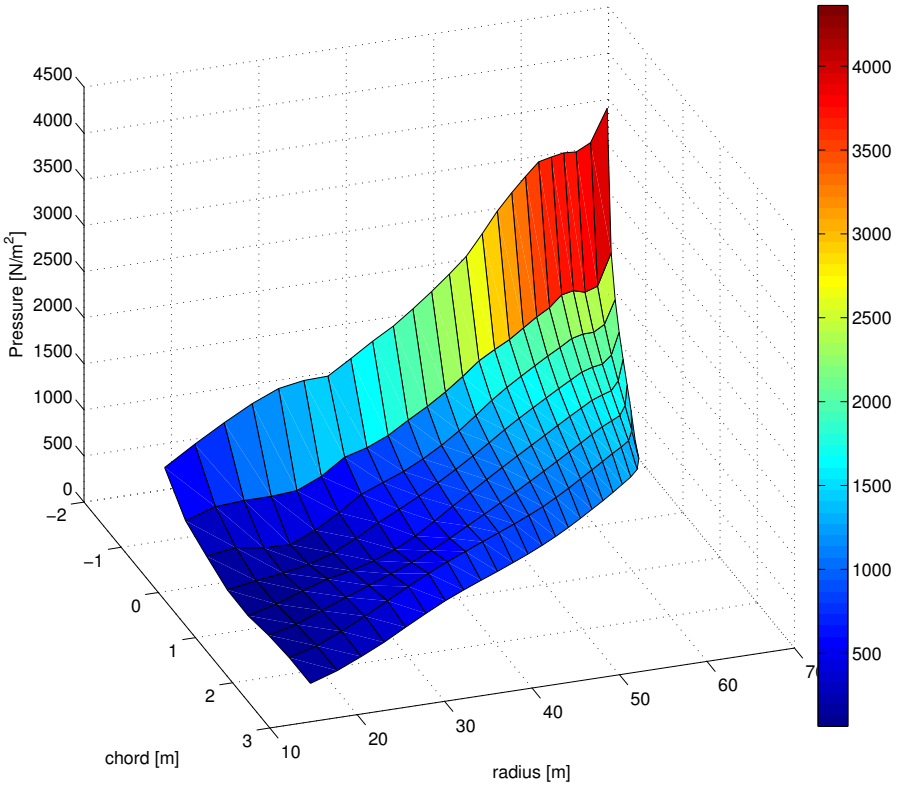

Aerodynamic Analysis of the NREL 5-MW Wind Turbine using Vortex Panel Method

Master's thesis in Fluid Mechanics

KATHARINA MÁIRÉAD SCHWEIGLER

Department of Applied Mechanics
Division of Fluid Dynamics
CHALMERS UNIVERSITY OF TECHNOLOGY
Gothenburg, Sweden 2012
Master's thesis 2012:17

MASTER'S THESIS IN FLUID MECHANICS

Aerodynamic Analysis of the NREL 5-MW Wind Turbine using Vortex Panel Method

KATHARINA MÁIRÉAD SCHWEIGLER

Department of Applied Mechanics
Division of Fluid Dynamics
CHALMERS UNIVERSITY OF TECHNOLOGY

Gothenburg, Sweden 2012

Aerodynamic Analysis of the NREL 5-MW Wind Turbine using Vortex Panel Method
KATHARINA MÁIRÉAD SCHWEIGLER

© KATHARINA MÁIRÉAD SCHWEIGLER, 2012

Master's thesis 2012:17
ISSN 1652-8557
Department of Applied Mechanics
Division of Fluid Dynamics
Chalmers University of Technology
SE-412 96 Gothenburg
Sweden
Telephone: +46 (0)31-772 1000

Cover:
Pressure distribution of a turbine blade of the NREL 5-MW wind turbine

Chalmers Reproservice
Gothenburg, Sweden 2012

Aerodynamic Analysis of the NREL 5-MW Wind Turbine using Vortex Panel Method
Master's thesis in Fluid Mechanics
KATHARINA MÁIRÉAD SCHWEIGLER
Department of Applied Mechanics
Division of Fluid Dynamics
Chalmers University of Technology

Abstract

The purpose of this study was to investigate if panel methods can be used to examine aerodynamic loads on wind turbine blades. Another aim was to find out the differences between the Lifting Surface Method, the Vortex Panel Method (a number of panels along the chord) and the Reduced Vortex Panel Method (one panel along the chord) when applied to horizontal axis wind turbines.

Panel methods use vortex filaments or rings to model the surface of a solid body and the wake behind the wind turbine. Therefore, a grid was laid on the blades and the wake. That way for every blade the influence of all wakes and blades was taken into account. In this thesis the wind profile was uniform. Furthermore, incompressible, frictionless flow was assumed.

The results for the NREL 5-MW wind turbine revealed that the Lifting Surface Method and the Reduced Vortex Panel Method produce similar force distributions along the blade (from root to tip). The forces obtained with the Vortex Panel Method are not only higher but also more accurate compared to Computational Fluid Dynamics, Blade Element Momentum and General Unsteady Vortex Particle data for the same blade.

The principal conclusion was, the Vortex Panel Method is a suitable tool to investigate the aerodynamic loads on horizontal axis wind turbines with three blades.

Keywords: Vortex Panel Method, Wind turbine, Aerodynamics, Thin Airfoil Theory, Lifting Surface Method, Induced velocity, NREL 5-MW

Zusammenfassung

Der Zweck dieser Arbeit war es, zu untersuchen, ob Panel Methoden zur Bestimmung der aerodynamischen Lasten auf Rotorblätter von Windenergieanlagen genutzt werden können. Ein weiteres Ziel dieser Arbeit war es, die Unterschiede zwischen der Lifting Surface Methode, der Vortex Panel Methode (einige Panele entlang der Sehne) und der Reduzierten Vortex Panel Methode (ein Panel entlang der Sehne), auf Windenergieanlagen mit horizontaler Achse angewandt, zu untersuchen.

Panel Methoden verwenden Vortexlinien oder -ringe, um die Oberfläche eines festen Körpers und die Wirbelschleppe hinter dem Windrad zu modellieren. Daher wurde ein Gitter auf den Rotorblättern und der Schleppe erstellt. Damit konnte der Einfluss von allen Wirbelschleppen und Blättern für jedes Blatt berücksichtigt werden. In dieser Arbeit war das Windprofil homogen. Desweiteren wurde inkompressible, reibungsfreie Strömung angenommen.

Die Ergebnisse für die NREL 5-MW Windturbine haben gezeigt, dass die Lifting Surface Methode und die Reduzierte Vortex Panel Methode ähnliche Kraftverteilungen entlang der Rotorblätter (von der Nabe bis zur Spitze) ergeben. Die Kräfte, die die Vortex Panel Methode lieferte, waren nicht nur höher, sondern auch genauer, verglichen mit Computational Fluid Dynamics, Blade Element Momentum und General Unsteady Vortex Particle Daten für das gleiche Rotorblatt.

Die wichtigste Schlussfolgerung war, dass die Vortex Panel Methode ein gutes Werkzeug ist, um die aerodynamischen Lasten auf Windenergieanlagen mit horizontaler Achse und drei Rotorblättern zu untersuchen.

Acknowledgements

First of all I would like to thank Professor Lars Davidson for kindly accepting me as a master's thesis student at the Division of Fluid Mechanics and for letting me feel welcome the whole time together with the Staff of the Division.
I would also like to thank Professor Martin Gabi for giving me the chance to work on this topic.

Very special thanks go to my supervisor Hamidreza Abedi for his support and guidance throughout this thesis. He has always given optimistic comments and constructive advice. Thanks to Christoffer Järpner and Ayyoob Zarmehri for their helpful ideas and the supply with CFD data.
Thanks to Pablo Mosquera Michaelsen for supporting me during the last weeks of my thesis in Germany. Mrs. Kölmel, thanks for always being so friendly and helpful with all formalities.

For financial support, I thank the Friedrich-Ebert-Stiftung, without whose help all of this would not have been possible.

My final words go to my family and friends. Without their support from Germany and during their stay in Sweden it would have been very hard to write this thesis abroad.

Nomenclature

Roman letters

ai	influence coefficient
b	span length
c	chord length
c_L	lift coefficient
i	grid node counter along chord
j	grid node counter along span
k	grid node counter along wake
l	variable along a vortex filament
n	normal
q	velocity
r	radius / distance from control point to one end of a vortex filament
u	velocity component in x-direction
v	velocity component in y-direction
w	velocity component in z-direction
Ai	influence coefficients matrix
AR	aspect ratio
F	force
L	lift
L'	lift per unit span
R	maximal radius

Greek letters

α	angle of attack
β	angle between two wake consecutive grid nodes in the wake
γ	vorticity, vortex strength or circulation of a single vortex element
ρ	density of air
ϕ	velocity potential
ω	rotation of a fluid
Γ	vortex strength distribution

Subscripts

b	body
eff	effective
i	induced
m	number of vortex rings
n	number of control points
nor	normal to rotor plane
rot	rotational
$tang$	tangential to rotor plane
$T.E.$	trailing edge
θ	tangential to vortex filament
∞	free stream

Abbreviations

BEM	Blade Element Momentum
CFD	Computational Fluid Dynamics
GENUVP	GENeral Unsteady Vortex Particle
NREL	National Renewable Energy Laboratory
RVPM	Reduced Vortex Panel Method
VPM	Vortex Panel Method

Contents

List of Figures

List of Tables

1 Introduction

1.1 Motivation

While renewable energies, especially wind power, become more and more important as a part of the energy mix of many countries the need for fast and reliable methods for the development of wind turbines becomes larger.

In the field of aerodynamics it is very important to determine the actual forces on wings and blades. Therefore it is vital to know the behaviour of the flow field surrounding them. Especially for wind turbines it is important to have an accurate load estimation for the blades, since they dictate the power outcome of the turbine.

So far the approach of the Blade Element Momentum (BEM) and Computational Fluid Dynamics (CFD) calculations are mainly used to model the flow field behind and around the wind turbine blades. Both methods have advantages: the BEM is easy to implement and since it is very fast it has low computational cost. CFD on the other hand delivers much more exact results.

Hence both advantages are very important for industrial purposes, a method that combines them is needed. That method could be a vortex method. It is faster than CFD [12] and it is able to handle more complicated cases than BEM [3], [14].

1.2 Objective

The objective of this thesis is to model the flow field around the NREL 5MW wind turbine using the vortex panel method. Different approaches of the vortex panel method have to be investigated throughout the thesis.

The results should be compared to CFD and BEM data and evaluated with respect to quality of the results and computation speed. Furthermore it should be understood what the limitations of the vortex panel method with respect to wind turbine modelling are.

1.3 Outline of the thesis

In this thesis first of all the terminology concerning wings and wind turbines is clarified in chapter *Fundamentals*. Additionally governing equations, assumptions and boundary conditions concerning panel methods are addressed. Finally the basic vortex methods (thin airfoil theory, lifting surface method and vortex panel method) are introduced in the end of the chapter.

In chapter *Method* the Vortex panel method is explained step by step, including the principle behind it and how it is applied to a wing or blade in a free stream.

Additionally the MATLAB procedure and models for the wind turbine and the wake behind the turbine are introduced.

In *Results* first the flow field around an airfoil and the pressure distribution on a 3-D wing are shown. Then the results for a single rotating wind turbine blade as well as a whole wind turbine are discussed. In the section *Validation* the results of the vortex panel method are compared to GENUVP [15], BEM and CFD data at different wind speeds and rotational velocities.

Finally conclusions are presented and future work is recommended.

2 Fundamentals

There are several simple methods that can be used to obtain the forces acting on a wind turbine blade during operation, e.g. analytical solutions, the thin airfoil theory, the lifting line theory or the vortex panel method. After the terminology concerning wind turbines has been introduced, all of them will be explained briefly in this chapter.

2.1 Terminology

First of all the nomenclature of an airfoil, a wing, a wind turbine blade and finally a wind turbine is introduced in this section.

a) Airfoil

An airfoil is the shape of a wing or a blade at its cross-section, as shown in figure 2.1.1. The heart of an airfoil is the camber line. It mainly defines the shape. The camber line is the line exactly at the middle between the upper and the lower surface of an airfoil. When constructing an airfoil the camber line is the first element to be drawn. Then thickness is added on both sides equally and perpendicular to the camber line. That gives the surface of the wing. The leading edge is at the part of the wing where the surface has the biggest curvature and the trailing edge is at the pointy edge of the airfoil. Both are exactly at the beginning and the end of the camber line. The chord connects the two ends of the camber line and is consequently the length of the airfoil.

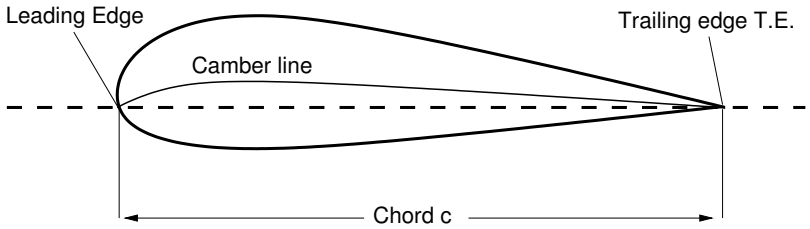

Figure 2.1.1: *Airfoil nomenclature*

b) Wing

A wing is always a 3-D geometry that consists of one or more airfoils which are distributed along the span (also called the width of the wing), see figure 2.1.2.

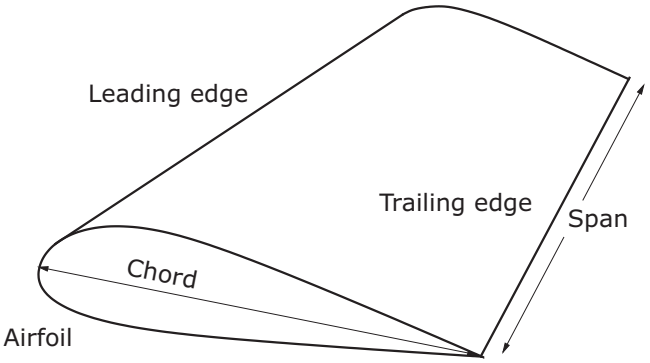

Figure 2.1.2: *Wing nomenclature*

c) Wind turbine blade

The wind turbine blade is similar to a wing, as can be seen in figure 2.1.3. It usually consists of many different airfoils that are distributed along the span. The pitch angle gives the change in angle of attack of the entire wing and the twist is the local change that can be different for every airfoil section.

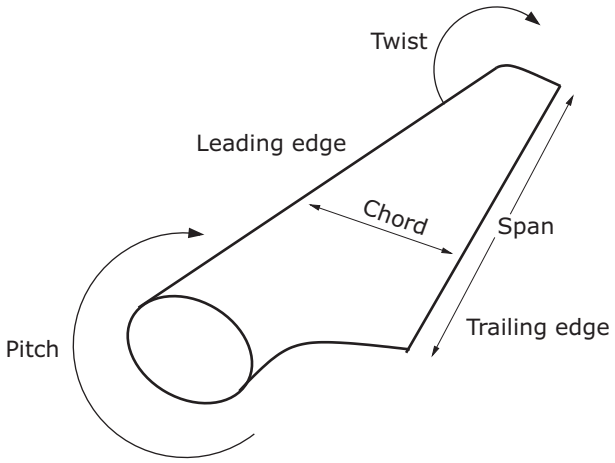

Figure 2.1.3: *Blade nomenclature*

d) Horizontal axis wind turbine

A wind turbine generally consists of a foundation, a tower and a hub to which a number of rotor blades are attached. In the case of a three bladed wind turbine the blades rotate around a horizontal axis with an angular distance of 120 degrees to each other. (See figure 2.1.4)

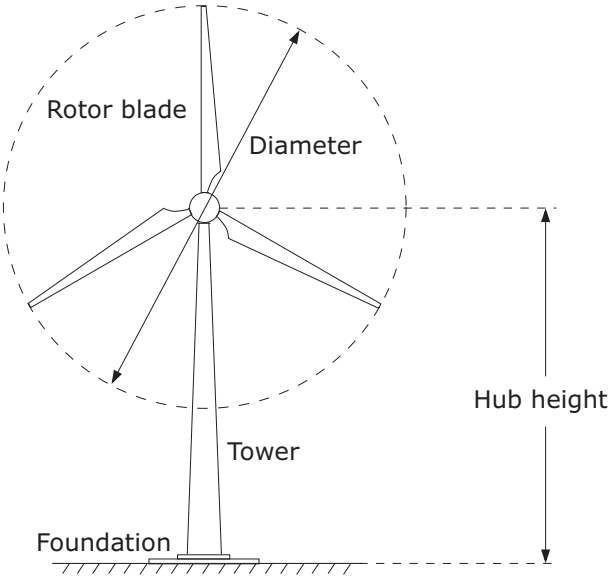

Figure 2.1.4: *Wind turbine nomenclature*

2.2 Lift

In order to analyse the behaviour of a solid body in a free stream it is important to know the surface force that it experiences due to the flow. As shown in figure 2.2.1, the component of the force that is perpendicular to the free stream is called lift, L, whereas the component in direction of the free stream is called drag, D. To obtain the lift of an airfoil section or wing analytically, one has to

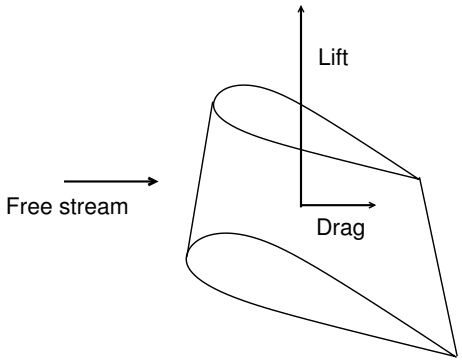

Figure 2.2.1: *Lift and Drag*

know the density of air, ρ, the chord length, c, the free stream velocity, q_∞ and the lift coefficient, c_L :

$$L = \frac{1}{2}\rho\, c\, q_\infty^2\, c_L \tag{2.2.1}$$

2.3 Governing equations

For the calculation of a flow field around a solid body the main equations of fluid flow theory have to be introduced. From the conservation of mass we get the continuity equation

$$\frac{\partial \rho u}{\partial x} + \frac{\partial \rho v}{\partial y} + \frac{\partial \rho w}{\partial z} + \frac{\partial \rho}{\partial t} = 0 \tag{2.3.1}$$

which can be reduced for an incompressible fluid ($\frac{\partial \rho}{\partial t} = 0,\ \nabla \rho = 0$):

$$\frac{\partial u}{\partial x} + \frac{\partial v}{\partial y} + \frac{\partial w}{\partial z} = \nabla \cdot \mathbf{q} = 0 \tag{2.3.2}$$

The velocity potential, ϕ, can be used to express the velocity as the gradient of ϕ. The velocity potential for irrotational flow can be applied to 3-D flows. Since it can be obtained by differentiating in the same direction as the velocities

$$\mathbf{q} = \nabla \phi \tag{2.3.3}$$

we can write the velocity components as

$$u = \frac{\partial \phi}{\partial x} \quad v = \frac{\partial \phi}{\partial y} \quad w = \frac{\partial \phi}{\partial z} \tag{2.3.4}$$

The rotation of a fluid is given by $\boldsymbol{\omega} = \hat{\mathbf{i}}\omega_x + \hat{\mathbf{j}}\omega_y + \hat{\mathbf{k}}\omega_z$ and can be denoted as the curl of $\mathbf{q}$:

$$\boldsymbol{\omega} = \frac{1}{2} \nabla \times \mathbf{q} \tag{2.3.5}$$

A useful tool to measure the rotation of a fluid element around itself as it moves in the flow field is the vorticity, γ, that is defined to be twice the rotation.

$$\boldsymbol{\gamma} = 2\boldsymbol{\omega} = \nabla \times \mathbf{q} \tag{2.3.6}$$

In contrast to the vorticity, the circulation, Γ, is not about the rotation of a fluid element, but about the enclosing path of the fluid element. (Note: this does not necessarily mean that the element moves on a circle.) Γ is the line integral of velocity around a closed curve in the flow,[9].

$$\Gamma = \oint_c \mathbf{q} \cdot d\mathbf{l} = \iint_S \nabla \times \mathbf{q} \cdot \mathbf{n}\, dS = \iint_S \boldsymbol{\gamma} \cdot \mathbf{n}\, dS \tag{2.3.7}$$

Furthermore the circulation is an important definition to calculate the lift of an airfoil. According to the Kutta-Joukowski theorem, lift is directly proportional to the circulation around a body

$$L' = \rho\, q_\infty\, \Gamma \tag{2.3.8}$$

where L', ρ, q_∞ are lift per span, air density and free stream velocity, respectively. Lift force acts always perpendicular to the free stream velocity and the vector notation gives:

$$\mathbf{F} = \rho\, \mathbf{q} \times \boldsymbol{\Gamma} \tag{2.3.9}$$

2.4 Assumptions

The flow field around the wing is assumed to be incompressible, inviscid and therefore irrotational (except at the core of a vortex filament).

$$\nabla \cdot \mathbf{q} = 0$$

$$\nabla \times \mathbf{q} = 0$$

This kind of flow is called potential flow. The free stream is considered as steady, uniform flow with the velocity vector $\mathbf{q}_\infty = (0, 0, w_\infty)$.

2.4.1 Consequences

A steady flow is independent of time and therefore the velocity vectors in the flow field must always be tangential to the streamlines. Concerning wind turbines the real wind profile is never uniform or steady. Therefore the computed power of a wind turbine does only apply to certain condition as fixed wind speed, not to real conditions.

Incompressible flow means in practice that the density is assumed to be constant. Besides simplifying the calculation (derivatives of density are zero) it means that the results are not 100 percent correct. Nevertheless, at low speeds, the variation in density of an airflow is very small and can be considered essentially incompressible, see [4].

Since the flow is also assumed to be inviscid there are no losses due to friction and the boundary layer between the stream and the surface of a solid body is extremely thin. This means that there are no viscous shear stresses and normal stresses due to viscosity acting on the body and the model does not predict the frictional drag of a body. The only stresses are normal to the surface and due to pressure. Although the results are usually still very close to experimental data, the model fails when it comes to stall conditions. In those cases the boundary layer can not be assumed to be very thin. In contrary it has to be added to the physical surface of the body and has therefore, depending on its thickness, a big influence on the angle of attack.

2.5 Boundary conditions

The Neumann boundary condition, that is also called direct boundary condition, states that on the surface of the solid body there can not be any velocity component normal to the surface.

$$\frac{\partial \phi}{\partial n} = 0$$

The second boundary condition is that the effect of the body does not reach for distance. It means at some distance to the body the velocity field should

be similar to the free stream upstream of the body. For an uniform free stream follows:

$$\lim_{r\to\infty} \nabla\phi_p = 0$$

where ϕ_p is the perturbation potential, respectively.

2.6 A vortex filament

A vortex filament is line of concentrated vorticity that induces a flow or velocity everywhere in its neighbourhood, depending on the the distance to the filament.

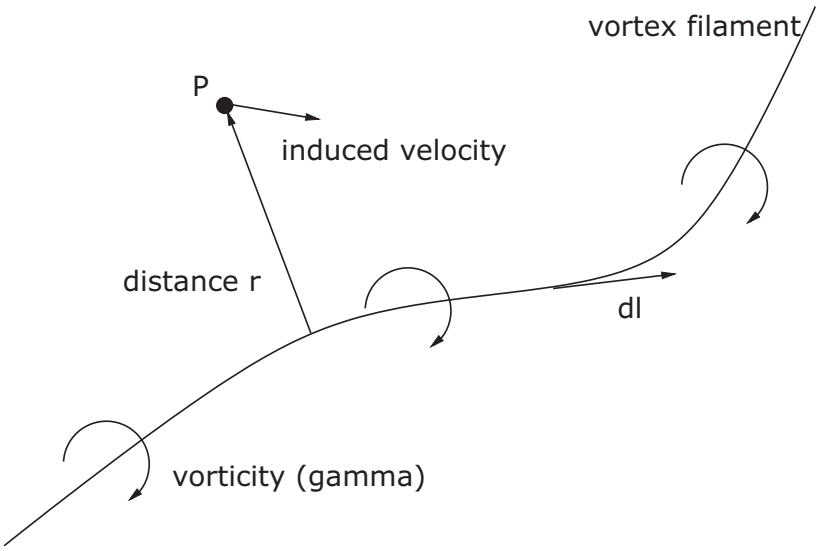

Figure 2.6.1: *Induction by a vortex filament*

Therefore the induced velocity $\mathbf{q}_\theta$ is

$$\mathbf{q}_\theta = \frac{C}{r} \tag{2.6.1}$$

where C is a constant and r is the distance from the vortex filament, respectively. Using equation 2.3.7 and applying it to a vortex filament gives

$$\Gamma = \oint_C \mathbf{q} \cdot d\mathbf{l} = \mathbf{q}_\theta \cdot 2\pi r \tag{2.6.2}$$

Therefore the rotational velocity of P is

$$q_\theta = \frac{\Gamma}{2\pi r} \tag{2.6.3}$$

The Helmholtz vortex theorem states that the strength of a vortex filament is constant along its length and that it cannot end within a fluid. That means it has to form a closed loop, as expressed by the circle integral.

Furthermore Kelvin's circulation theorem declares that the circulation around a closed curve formed by a set of contiguous fluid elements remains constant as the fluid elements move. [2]

$$\frac{D\mathbf{\Gamma}}{Dt} = 0 \tag{2.6.4}$$

2.7 Thin airfoil theory

This theory is used to obtain forces and pressure distributions due to lift of 2-D airfoils in incompressible inviscid flow. The airfoil is reduced to the camber line and therefore to zero thickness. This is possible, if only the lifting problem is

Figure 2.7.1: *Vortex distribution along the camber line*

addressed. Here drag and pressure difference along the chord are not discussed. Additionally a small angle approximation is made. This leads to the simplification that airfoil sections (with a small asymmetry between upper and lower camber) can be modelled as straight lines. To satisfy the boundary condition of zero velocity

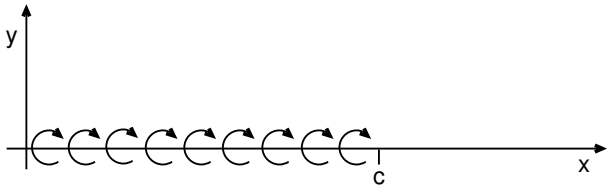

Figure 2.7.2: *Vortex distribution along the camber line on the x-axis*

component normal to the surface of the wing, a continuous distribution γ(x) of vortices is placed along the camber line, as shown in figures 2.7.1 and 2.7.2. These vorticities can be compared to a force field that induces a velocity component perpendicular to the camber line. Since this induced velocity cancels out with

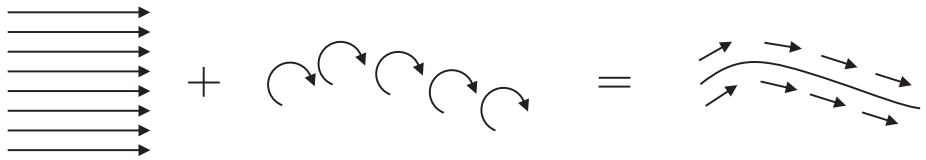

Figure 2.7.3: *Flow about a distribution of vorticities along the mean camber line placed in a uniform stream[7]*

the normal component of the free stream, the resolving flow does now follow the wings surface, see figure 2.7.3. For more detailed explanation see figure 3.1.2.

The distribution of the vorticities can be used to obtain the lift per span L':

$$L' = \rho \, q_\infty \int \gamma(x) \, dx \tag{2.7.1}$$

2.8 Lifting surface method

In order to obtain the lift of a finite wing at a given angle of attack and free stream velocity, the model of a lifting line can be used. This method uses vortex filaments to model the influence of the body and the wake on the free stream.

Therefore a bound vortex is placed at $\frac{1}{4}$ of the cord behind the leading edge along the span of the wing. Additionally two trailing vortices starting at both ends of the bound vortex and leaving the wing in chord wise direction simulate the wake behind the wing (see figure 2.8.1). The wake is the region downstream of an object in a free stream that differs from the free stream. It is caused by the stream flowing around the object. Trailing vortices are mostly caused by pressure differences. On both ends of a wing the higher pressure zone that is built under the wing meets the lower pressure side from above the wing. That difference leads to trailing vortices and therefore a wake roll-up. Together they form a so called

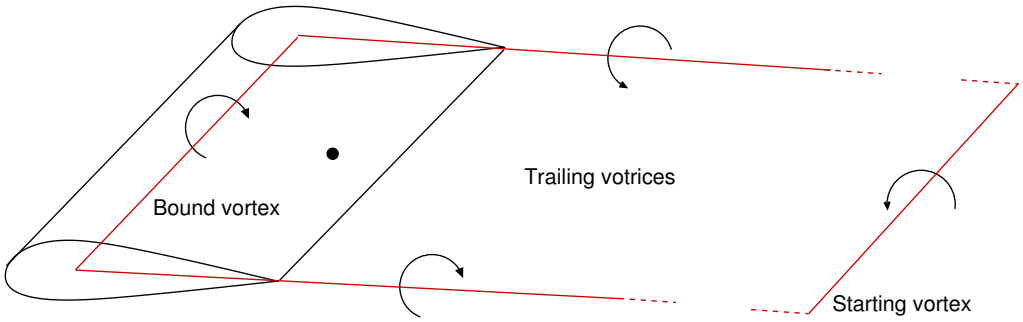

Figure 2.8.1: *Horseshoe model for finite wing*

"horseshoe vortex" of constant strength, Γ. Although the original theory states that vortices can only exist in closed loop, the influence of the part connecting the two trailing vortices, the starting vortex, can be neglected, see figure 2.8.2. That is only possible for steady state conditions, where the starting vortex has already moved very far downstream. Lift therefore is obtained as:

$$L = \rho \, b \, q_\infty \, \Gamma \tag{2.8.1}$$

Where ρ is the density of the fluid, b the span length, q_∞ the free stream velocity and Γ the strength for the bound vortex. Since the results of a single horseshoe vortex do only represent a model for 2-D airfoil sections, it is mandatory to divide the lifting line in many small bound vortices to obtain results that are valid for 3-D wings, as shown in figure 2.8.2. This method was first introduced by Ludwig Pradtl and is therefore called "Prandtl's lifting line method" [9]. Trailing vortices

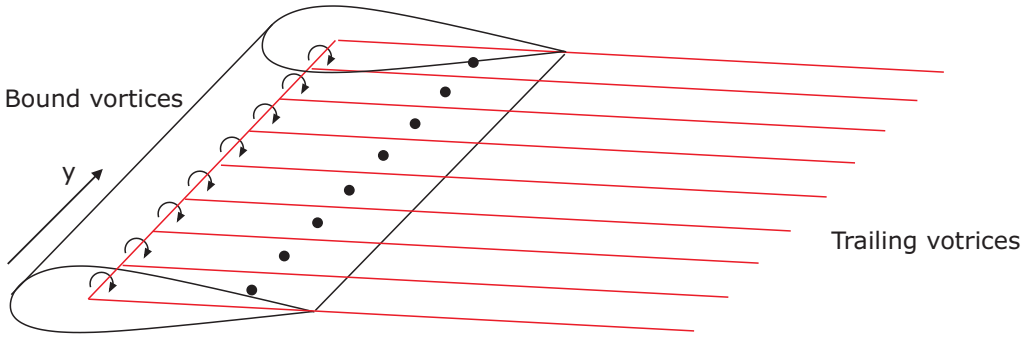

Figure 2.8.2: *Lifting line model consisting of many horseshoe vortices*

that are not on one of the two sides of a wing are only caused when there is a pressure difference between two sections of the wing due to a change of the wing profile or the free stream velocity, i.e. if $\frac{d\Gamma}{dy} \neq 0$.

2.9 Vortex Panel Method

The vortex panel method is a method for computing ideal flows e.g. over airfoils. It is a technique for solving incompressible potential flow over 2-D and 3-D geometries and can be seen as a combination of lifting surface method and thin airfoil theory. The vortex panel method combines the discretization along span and chord and therefore much more accurate results than with only one of the two methods can be achieved.

Consequently, an airfoil surface is divided into piecewise panels, as shown in figure 2.9.1. To reduce the computational effort the panels can also be placed on the camber surface of the wing, see figure 2.9.2. Since the panel method is based on the thin airfoil theory, here the thickness of the wing has no contribution to the lift. Figure 2.9.3 shows how vortex rings of strength γ are placed on each panel.

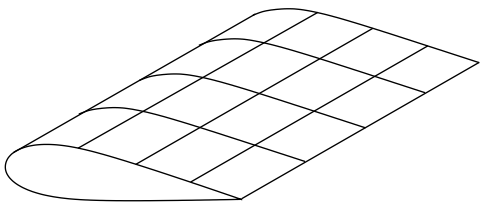

Figure 2.9.1: *Wing surface divided into panels*

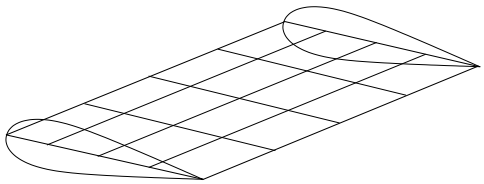

Figure 2.9.2: *Wing camber surface divided into panels*

Control points are placed in the center of each body panel. At those positions the boundary condition of zero flow perpendicular to the panel is applied, see below. Additionally the wake is modelled with another set of vortex rings behind the trailing edge of the wing. Since they do not represent a solid body, those vortex rings have no control point in the center. The exact procedure of using the vortex panel method to model a wing in ideal flow is explained in the chapter "Method".

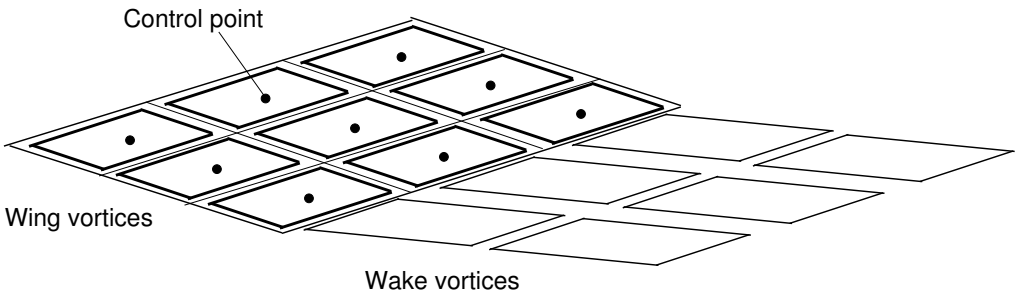

Figure 2.9.3: *Vortex ring on a flat wing and its wake*

2.10 Induced velocity

To determine the actual forces on wind turbine blades it is mandatory to know the exact velocity vectors of the flow field. Therefore it is necessary to know the real angle of attack. It consists of the geometric angle of attack and the induced angle. The induced angle can be obtained using the velocity component induced by the wake.

The induced velocity or down-wash velocity, $\mathbf{q_i}$, is the velocity produced by the wake behind the wing. Depending on the wake shape it has a larger or smaller effect on the angle of attack. Since the lift of a wing is proportional to the angle of attack it is mandatory to use the exact/real angle of attack: the effective angle of attack α_{eff}. It can be obtained by subtracting the induced from the geometric angle of attack.

$$\alpha_{eff} = \alpha_{geo} - \alpha_i \tag{2.10.1}$$

Figure 2.10.1 shows the nomenclature of the introduced angles. Assuming a

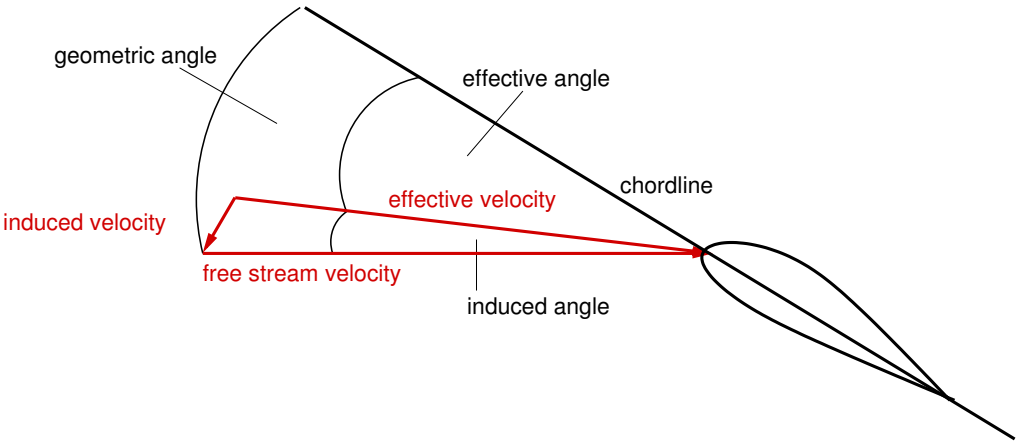

Figure 2.10.1: *Angle of attack nomenclature*

horizontal free stream velocity the induced velocity is pointing mainly downwards, which is the reason for its name "down-wash velocity"[5]. This velocity decreases the real angle of attack as shown in figure 2.10.1.

Furthermore the lift, which is always perpendicular to the effective velocity,

does not point straight up, but slightly in the direction of the free stream velocity. Therefore the lift in vertical direction is reduced and the drag is increased (see figure 2.10.2).

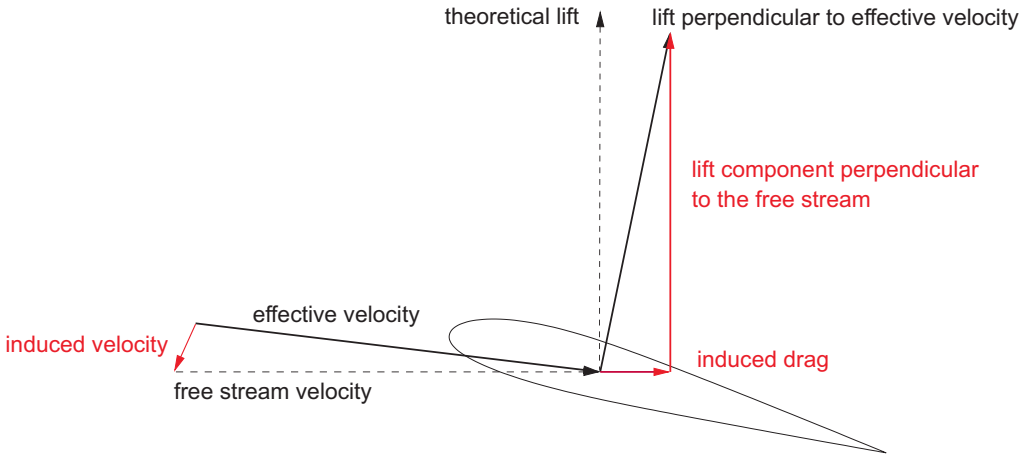

Figure 2.10.2: *Decreased lift due to induced velocities*

Especially the analytical solution for lift depends on the exact (effective) angle of attack:

2D-airfoil:

Using equation2.2.1 and substituting c_L with $2\pi\alpha$ we get

$$L = \alpha_{eff}\,\pi\,\rho\,c\,q_\infty^2 \tag{2.10.2}$$

where c is the chord length of the wing and $\mathbf{q}_\infty$ the free stream velocity.

3-D wing:

$$L = \alpha_{eff}^2\,\pi\,\rho\,c\,{q_\infty}^2\,\frac{AR}{AR+2} \tag{2.10.3}$$

Where AR is the aspect ratio of the wing and can be obtained as:

$$AR = \frac{span^2}{area\ of\ airfoil\ section} \tag{2.10.4}$$

For a rectangular planform that would be:

$$AR = \frac{b^2}{c \cdot b} = \frac{b}{c} \tag{2.10.5}$$

where b is the span length and c the chord length of a wing.

3 Method

3.1 Vortex panel method - step by step

First of all, as mentioned in section 2.9, the camber surface has to be divided into panels. Then vortex rings and control points are placed on each panel. An example of a vortex panel is given in figure 3.1.1. A closed vortex ring of constant strength γ and a control point are placed on the panel. The direction of the circulation follows the right-hand rule. Those vortex rings are used to model

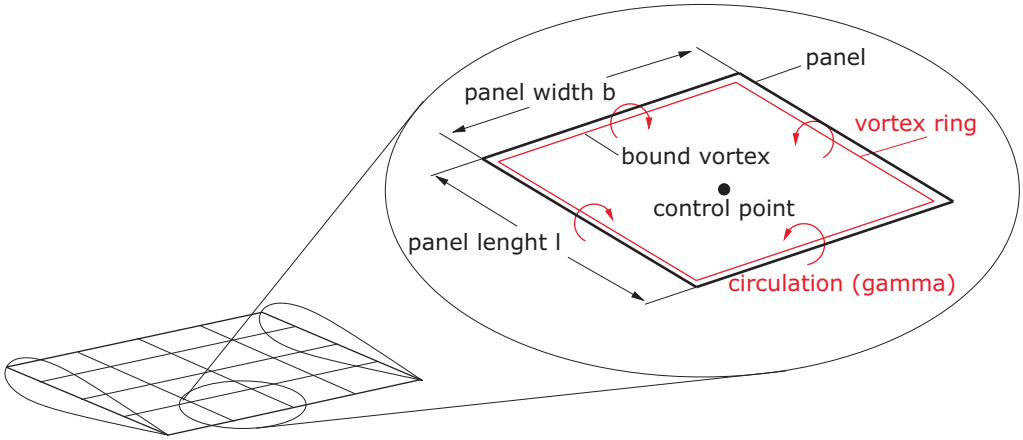

Figure 3.1.1: *Vortex panel nomenclature*

the wings physical surface. All vortex rings induce a velocity component at the control point in the center of each vortex ring. Here, the Neumann boundary condition of zero velocity component normal to the surface is applied. Therefore the following equations result:

$$\mathbf{q_{eff}} = \mathbf{q_\infty} + \mathbf{q_i} \tag{3.1.1}$$

$$\mathbf{q_i} = \mathbf{q_{eff}} - \mathbf{q_\infty} \tag{3.1.2}$$

As shown in figure 3.1.2 an induced velocity $\mathbf{q_i}$ has to be added to the free stream velocity $\mathbf{q_\infty}$ in order to gain an effective velocity $\mathbf{q_{eff}}$ that is purely parallel to the wings surface. Therefore the vortex panel method is based on the calculation of the of the induced velocities at the control points. For the velocity induced by a vortex filament holds:

$$d\mathbf{q_i} = \frac{\gamma}{4\pi} \frac{d\mathbf{l} \times \mathbf{r}}{\mid \mathbf{r} \mid^3} \tag{3.1.3}$$

Equation 3.1.3 is derived from the Biot-Savart Law and shows that the induced velocity depends on the strength of the vortex filament and its distance r. [9]

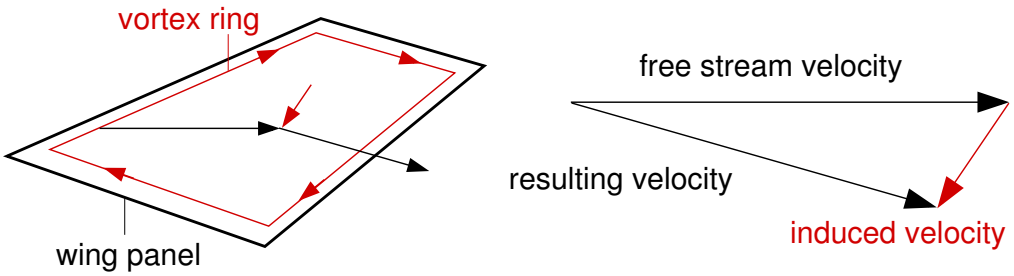

Figure 3.1.2: *Vector summation on a vortex panel in a free stream*

Hence the induced velocity is given by the integral along the whole vortex ring.

$$\mathbf{q_i} = \frac{\gamma}{4\pi} \int_c \frac{\mathbf{r} \times d\mathbf{l}}{|\ \mathbf{r}\ |^3} \tag{3.1.4}$$

Since the vortex rings are quadratic elements, the easiest way to get $\mathbf{q_i}$ is to calculate the induced velocity of each vortex filament separately. Given that a

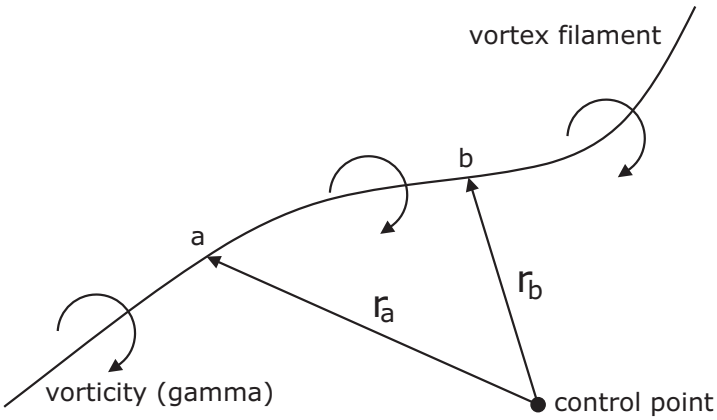

Figure 3.1.3: *Local vectors* $\mathbf{r_a}$ *and* $\mathbf{r_b}$ *from a control point to an arbitrary vortex filament*

and b are start- and endpoints on a filament and $\mathbf{r_a}$ and $\mathbf{r_b}$ are the vectors from the control point to a and b, see figure 3.1.3, the following equation results:

$$\mathbf{q_1} = \frac{\gamma}{4\pi} \frac{(r_a + r_b)(\mathbf{r_a} \times \mathbf{r_b})}{r_a r_b (r_a r_b + \mathbf{r_a} \cdot \mathbf{r_b})} \tag{3.1.5}$$

Repeating this procedure for the remaining three filaments, we consequently get $\mathbf{q_2}$, $\mathbf{q_3}$ and $\mathbf{q_4}$. $\mathbf{q_i}$ can therefore be obtained with

$$\mathbf{q_i} = \mathbf{q_1} + \mathbf{q_2} + \mathbf{q_3} + \mathbf{q_4} \tag{3.1.6}$$

As a simple example of how the vortex panel method is applied to a wing, a 3-D symmetric wing at an arbitrary angle of attack α is used. The wing is divided into nine vortex panels as can be seen in figure 3.1.4. Additionally there are six wake panels shown in the figure. The grid nodes are numbered with j as a counter

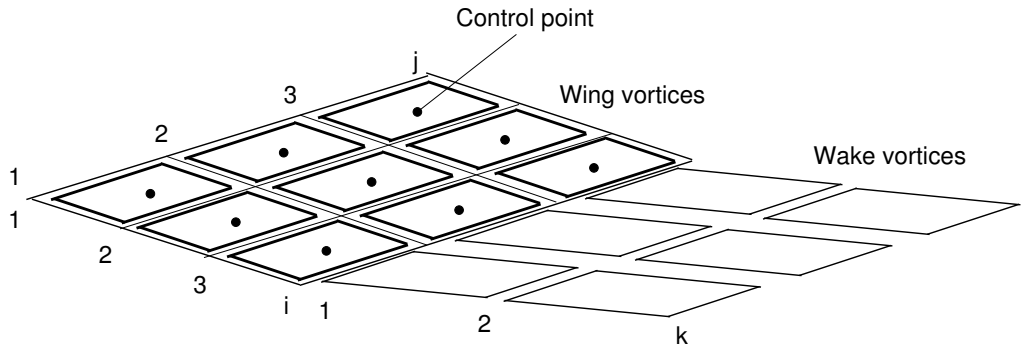

Figure 3.1.4: *Vortex panels distributed on the camber surface of a symmetric wing*

along the span of the wing, i as a counter along the camber line and k from the trailing edge of the wing to the end of the wake.

Calculating the induced velocities for $\gamma = 1$, the influence coefficients ai can be obtained. They represent the influence of every vortex ring of wing and wake to each control point, as figure 3.1.5 shows for one control point.

$$ai = \mathbf{q_i}(\gamma = \mathbf{1}) \tag{3.1.7}$$

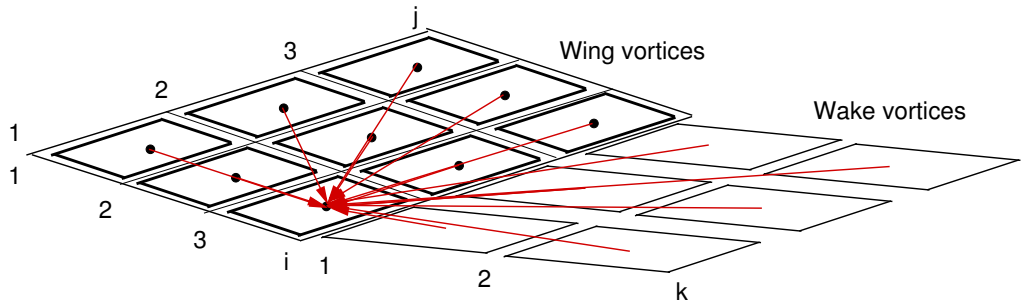

Figure 3.1.5: *Influence of the vortex rings on a control point*

Using the Neumann boundary condition, the following equation for a solid body in a uniform flow field can be obtained

$$\frac{\partial(\phi_b + \phi_\infty)}{\partial n} = 0 \tag{3.1.8}$$

and therefore

$$\nabla(\phi_b + \phi_\infty) \cdot \mathbf{n} = 0 \tag{3.1.9}$$

or

$$(\mathbf{q_i} + \mathbf{q}_\infty) \cdot \mathbf{n} = 0 \tag{3.1.10}$$

This means that the normal component of the free stream velocity, $\mathbf{q}_\infty \cdot \mathbf{n}$, and the normal component of the induced velocity, $\mathbf{q_i} \cdot \mathbf{n}$, have to have the opposite magnitude in order to cancel each other out. The free stream velocity can be moved to the right-hand side of the equation:

$$\mathbf{q_i} \cdot \mathbf{n} = -\mathbf{q}_\infty \cdot \mathbf{n} \tag{3.1.11}$$

The induced velocity at one control point consists of the influence coefficients and the vortex strengths of all blade and wake vortex rings,

$$\mathbf{q_{i1}} = \mathbf{ai_n}\ \boldsymbol{\gamma_n} \tag{3.1.12}$$

where n is the number of vortex rings ($(j-1)(i+k+2)$). Substituting equation 3.1.12 into equation 3.1.11 we get

$$\mathbf{ai_n}\,\mathbf{n}\cdot\boldsymbol{\gamma_n} = -\mathbf{q_{\infty 1}}\mathbf{n} \tag{3.1.13}$$

Expanding the equation for all control points (the total number of control points is m ($(j-1)(i+1)$)) all influence coefficients can be stored in the matrix $Ai_{m,n}$.

$$\mathbf{Ai_{m,n}} = \begin{pmatrix} a_{1,1} & a_{1,2} & \cdots & a_{1,n} \\ a_{2,1} & a_{2,2} & \cdots & a_{2,n} \\ \vdots & \vdots & \ddots & \vdots \\ a_{m,1} & a_{m,2} & \cdots & a_{m,n} \end{pmatrix} \tag{3.1.14}$$

$$\mathbf{q_{i\,m,n}} = \mathbf{Ai_{m,n}}\ \boldsymbol{\gamma_n} \tag{3.1.15}$$

With equation 3.1.15 the solution equation can be rewritten as:

$$\mathbf{Ai_{m,n}}\ \mathbf{n}\cdot\boldsymbol{\gamma_n} = -\mathbf{q_{\infty\,m}}\cdot\mathbf{n} \tag{3.1.16}$$

$$\begin{pmatrix} a_{1,1} & a_{1,2} & \cdots & a_{1,n} \\ a_{2,1} & a_{2,2} & \cdots & a_{2,n} \\ \vdots & \vdots & \ddots & \vdots \\ a_{m,1} & a_{m,2} & \cdots & a_{m,n} \end{pmatrix} \begin{pmatrix} \gamma_1 \\ \gamma_2 \\ \vdots \\ \gamma_n \end{pmatrix} = - \begin{pmatrix} q_{\infty,1} \\ q_{\infty,2} \\ \vdots \\ q_{\infty,m} \end{pmatrix} \tag{3.1.17}$$

This gives a set of linear equations that can not be solved for all $\boldsymbol{\gamma}$ of body and wake because there are still to many unknowns. Equation 3.1.17 contains only the equations for the body $\boldsymbol{\gamma}$ but the wake and body depend on each other. That problem is solved using the Kutta condition.

The Kutta condition applies to the vortex panel method, the thin airfoil theory as well as the lifting line theory. It manly states that the flow should leave the trailing edge of a wing smoothly. To satisfy that condition the vorticity γ at the trailing edge $T.E.$ has to be zero.

$$\gamma_{T.E.} = 0 \tag{3.1.18}$$

For the vortex panel method this is applied by setting the strength of the first wake vortex ring equal to the strength of the last vortex ring on the wing. That way they will always cancel out at the trailing edge. Therefore, for each wake vortex ring, an equation is added that states that the strength is the same as the one of the wing panel at the trailing edge. Now the set of equations can be solved

for all $\boldsymbol{\gamma}$. With the obtained values of the circulation and equation 2.3.8 forces on the wing can be calculated.

In order to apply the vortex panel method to a wind turbine important changes have to be made. A wind turbine is a rotating system with a non-homogeneous velocity distribution along the turbine blades. Therefore the free stream velocity is now substituted by the vector addition of the free stream velocity and the rotational velocity. Effects of fictitious forces as the centrifugal and Coriolis force are neglected here.

$$\mathbf{q}_{\infty+rot} = \mathbf{q}_{\infty} + \mathbf{q}_{rot} \tag{3.1.19}$$

Furthermore most wind turbines have more than one blade. The NREL 5MW wind turbine has 3 blades of the same kind. This means that the wake behind a wind turbine, that was shed by blade one, does not only affect blade one, but also blades two and three and vice versa. Additionally the blades affect each other. In order to get the correct induced velocities for every control point on each blade all vortex rings of all blades and their wakes have to be included in the solution matrix. Then induced velocities can be calculated by using the influence coefficients of all wake vortex rings and their calculated strengths.

With the equation for the effective velocity 3.1.1 and the Kutta-Joukowski theorem the forces on the rotor blade can be calculated for every control point:

$$\mathbf{F} = \rho \cdot \mathbf{q}_{eff} \times \boldsymbol{\Gamma} \tag{3.1.20}$$

where $\boldsymbol{\Gamma}$ is the difference in vortex strength of each vortex ring and its neighbour in direction to the leading edge.

$$\Gamma_n = \gamma_n - \gamma_{n-1} \tag{3.1.21}$$

Since the first panel at the leading edge has no neighbour in downstream direction the value of Γ_n is equal to its vortex strength γ_n.

In this thesis two forces are differentiated: the force normal to the rotor plane (usually in free stream direction) F_{nor} and the force tangential to the rotor plane (in rotational direction) F_{tang}, see figure 3.1.6.

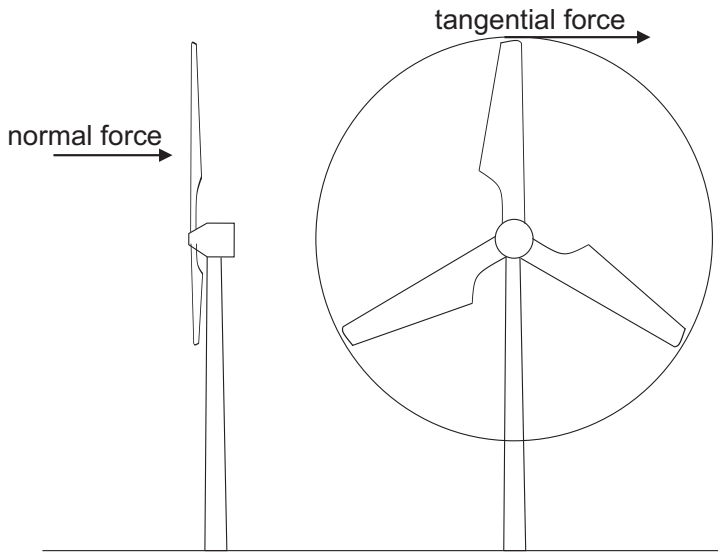

Figure 3.1.6: *Normal and tangential forces with respect to the rotor plane*

3.2 Implementation in MATLAB

The vortex panel method was implemented in MATLAB as shown in figure 3.2.1. First of all a geometry has to be loaded from file or in case of a symmetric wing, the four corners of the wing have to be assigned. Then important parameters such as grid size, wake length and the maximal residual have to be set. Now a grid can be generated on the wings/blades camber surface. Then the initial shape of the wake is prescribed.

Furthermore control points are set in the center of each wing vortex ring. At these points the condition of zero velocity component normal to the surface is applied later on in the code. Therefore normal vectors have to be obtained at every control point.

The next steps have to be within the iteration loop since the values of the parameters, especially the ones connected to the wake, can change with every iteration. With the information about the position of the blade and wake vortices the influence coefficients can be obtained and gathered in the matrix **Ai**. For each control point on the wing and each node in the wake grid the influence of all vortex rings is taken into account. The normal component of these influence coefficients multiplied by the strength of each vortex ring gives the left-hand side (lhs) of the equation:

$$\mathbf{Ai} \cdot \mathbf{n}\, \boldsymbol{\gamma} = -\mathbf{q}_{\infty+\mathbf{rot}} \cdot \mathbf{n} \tag{3.2.1}$$

The right-hand side (rhs) is obtained by deriving the normal component of the free stream and rotational velocity at each control point.

Then the equation is solved for the vorticity vector $\boldsymbol{\gamma}$, which is the key point of the code. With the vortex strengths, the effective and induced velocities are

found quickly.

$$\mathbf{q_i} = \mathbf{Ai} \cdot \boldsymbol{\gamma} \tag{3.2.2}$$

Knowing those it is now possible to calculate the new position of the wake (depending on the chosen wake shape, see section 3.3.2). These actions are repeated till the position of the wake does not change any more, according to the accepted residual.

Now the pressure distribution, lift, normal and tangential forces can be calculated and plotted.

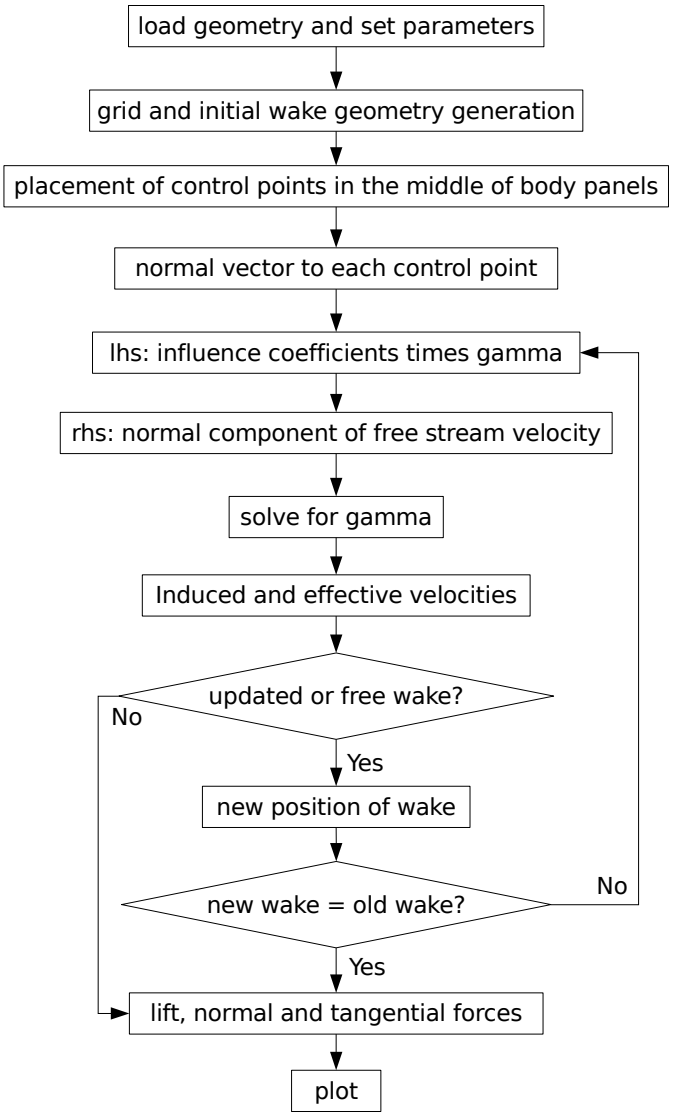

Figure 3.2.1: *Implementation in MATLAB*

3.3 Model used in MATLAB simulation

3.3.1 Wind turbine

As reference wind turbine the NREL 5MW has been used because there has been a lot of research on the blade in the past and therefore it is suitable for comparison. The following table, table 3.3.1, describes the blade geometry. The first column is the radial distance from the center r, the second column is the chord length at that radius, the third column is the twist and the last column is the airfoil type used at that radius. The airfoil shapes can be found in Appendix. A.2.

Table 3.3.1: Specification of NREL 5MW turbine blade [8]

r [m]	c [m]	Twist [deg]	Airfoil
11.75	4.557	13.308	DU40_A17
15.85	4.652	11.480	DU35_A17
19.95	4.458	10.162	DU35_A17
24.05	4.249	9.011	DU30_A17
28.15	4.007	7.795	DU25_A17
32.25	3.748	6.544	DU25_A17
36.35	3.502	5.361	DU21_A17
40.45	3.256	4.188	DU21_A17
44.55	3.010	3.125	NACA64_618
48.65	2.764	2.319	NACA64_618
52.75	2.518	1.526	NACA64_618
56.16	2.313	0.863	NACA64_618
58.90	2.086	0.370	NACA64_618
61.63	1.419	0.106	NACA64_618

The coordinate system is placed on one blade of the wind turbine as can be seen in figure 3.3.1. The x-axis is along the chord with zero pitch and twist, the y-axis is along the span from the hub to the tip of the blade and the z-axis follows the right-hand-rule. The free stream is in positive z-direction.

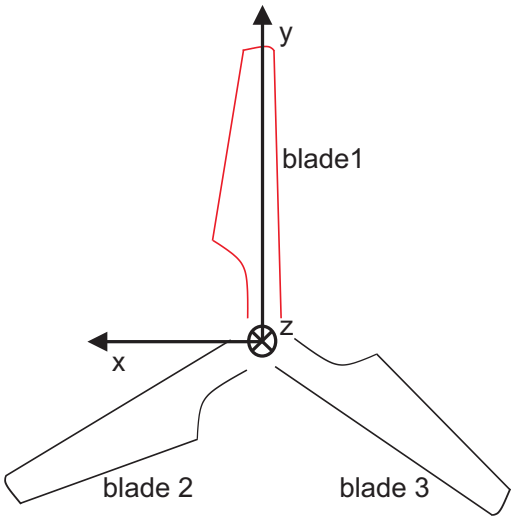

Figure 3.3.1: *Coordinate system used in the MATLAB code*

Figure 3.3.2 shows the three rotor blades as used in the calculation and figure 3.3.3 gives an overview about the setup simulated in the code.

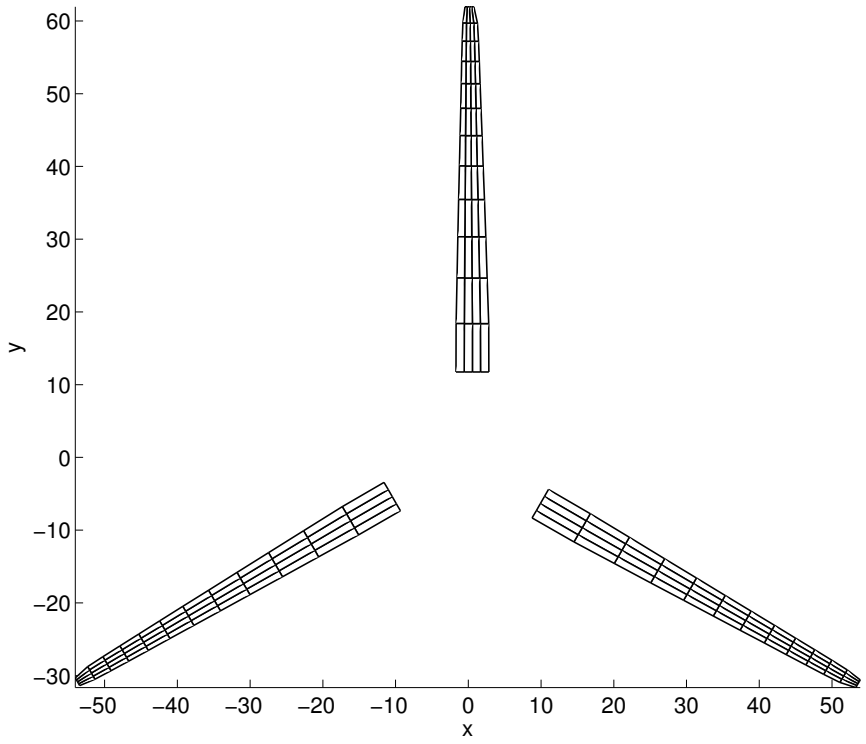

Figure 3.3.2: *Rotor geometry of NREL 5MW wind turbine*

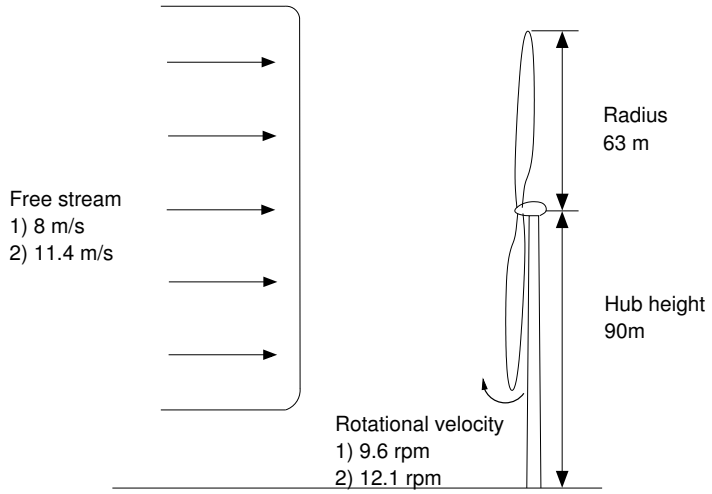

Figure 3.3.3: *Setup: wind turbine in a uniform free stream*

3.3.2 Wake shapes

The shape of the wake behind the wind turbine is a crucial factor in the calculation of the power outcome. There are several different models for a wake:

a) prescribed helical wake

The wake shape is set at the beginning and does not change during the computation. It is described by the following equation:

$$\begin{pmatrix} x \\ y \\ z \end{pmatrix} = \begin{pmatrix} r \cdot \sin(\frac{t \cdot rpm \cdot k \cdot \pi}{30}) \\ r \cdot \cos(\frac{t \cdot rpm \cdot k \cdot \pi}{30}) \\ t \cdot q_\infty \cdot k \end{pmatrix} \tag{3.3.1}$$

where k is the number of wake nodes, t is the time step and r the radius along the blade.

b) updated helical wake

The wake shape is set at the beginning and changes during the computation. After each iteration the new position of the wake grid points is calculated by adding the induced velocity at the blade to the free stream velocity:

$$\begin{pmatrix} x \\ y \\ z \end{pmatrix} = \begin{pmatrix} r \cdot \sin(\frac{t \cdot rpm \cdot k \cdot \pi}{30} + \frac{t \cdot q_{induced}(u,v) \cdot \pi}{180}) \\ r \cdot \cos(\frac{t \cdot rpm \cdot k \cdot \pi}{30} + \frac{t \cdot q_{induced}(u,v) \cdot \pi}{180}) \\ t \cdot (q_\infty + q_{induced}(w)) \cdot k \end{pmatrix} \tag{3.3.2}$$

c) free wake

The free wake is modelled differently. There is no prescribed wake at the beginning. In contrary, there is nearly no wake. Only at the first time step a row of vortex panels is placed at the trailing edge of the turbine blade. Then induced velocities are calculated for the control points on the blade as well as

the grid point of the wake. With the information of the induced velocity and the free stream velocity at all wake grid points, they can be moved according to the combined velocity vectors. That way the wake moves freely behind the wind turbine.

4 Results

In this chapter the results of the above introduced methods applied on three different cases are discussed. The first case is a 3-D wing. That means that the results are valid for a wing with a finite wing span. A single turbine blade that is rotating around a horizontal axis formulates the second case and a full scale wind turbine with three blades is used in case three. Furthermore these results are validated using GENUVP, CFD and BEM data.

4.1 3-D wing

a) Visualization of the flow field

Using the vortex panel method it is possible to obtain the velocity vectors of the flow field around a wing. As an example the flow field around a symmetric wing in a uniform flow field is shown in figure 4.1.1. The wing is modelled by the chamber line (blue) at a small angle of attack. The prescribed wake is shown in red. It can be seen how the flow follows the surface of the wing. Further away from the wing the disturbance caused by the wing goes to zero. This is consistent with experimental data of wings in a flow channel. However, in the region close to the camber line of the wing induced velocities can only be determined at the control points. At other points the result for the velocity vector is wrong as can be seen at the arrow pointing downwards from the camber line.

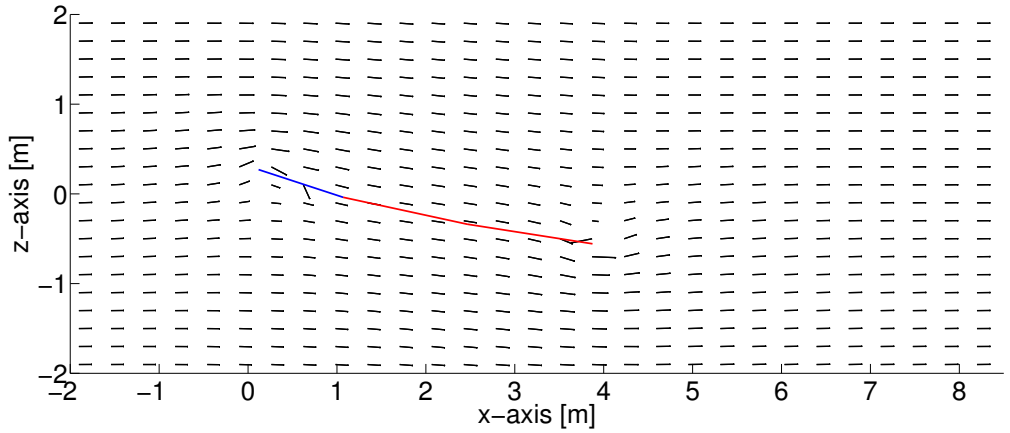

Figure 4.1.1: *Visualization of the flow field around a symmetric wing*

The wing used in this calculation could be any symmetric wing. An example would be the NACA 0012 as shown in figure 4.1.2 [13].

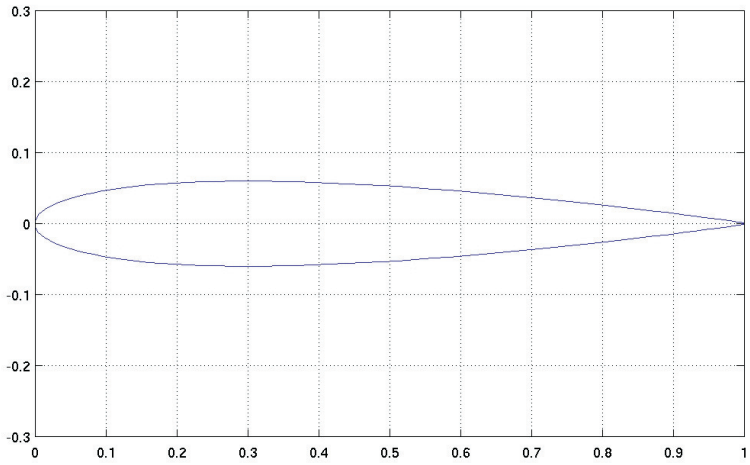

Figure 4.1.2: *Airfoil section NACA 0012*

b) Pressure distribution

The pressure distribution can be plotted over the wing surface since relative pressure values are available at every control point by dividing the force vector of the control point through its panel area. The pressure difference is the difference in pressure of upper and lower wing surface normal to the camber line.

Figure 4.1.3 shows the pressure distribution of a symmetric wing at $\pi/16$ radians angle of attack and 10 m/s wind speed. The span of the wing is 10 meters and the chord measures 1 meter. The same parameters are used for figure 4.1.5. The only difference is that here NACA profile N2414 is used, which is slightly asymmetric, see figure 4.1.4. That means that the chamber line is not a straight line, but has a certain curvature.

In both plots of the pressure distribution it can be seen that the difference in pressure of upper and lower surface of the wing is the highest in the middle close to the leading edge. It trends to zero at both sides of the wing and at the trailing edge.

Since there are no control point exactly at the edges, the plot does not show any zero values at the four edges. From leading to trailing edge the pressure drops quickly. From the middle to one of the sides of the wing the pressure drop can be expressed as inverse parabolic.

The difference between a symmetric and an asymmetric wing is the maximal value of the pressure difference. The pressure difference of the asymmetric

wing is more equally distributed and has therefore a smaller maximum. This can be explained with the smoother flow guidance of the bent camber line.

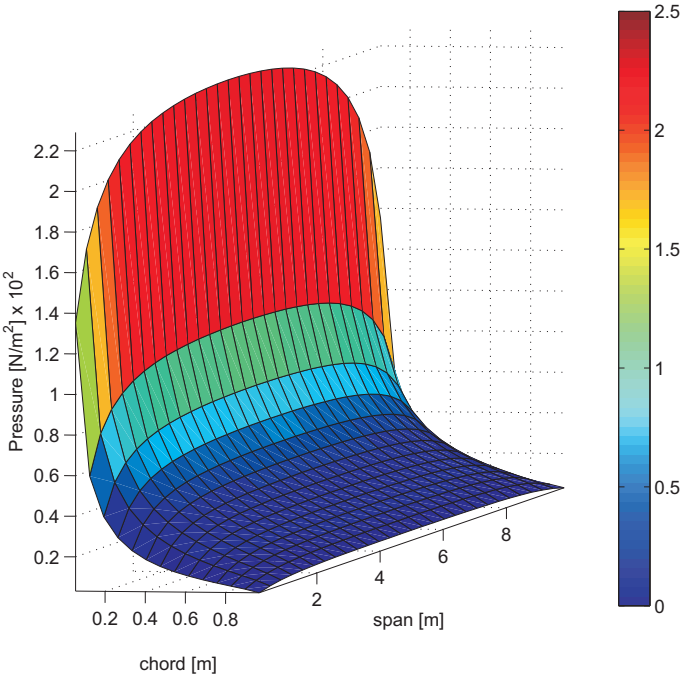

Figure 4.1.3: *Pressure distribution, symmetric wing*

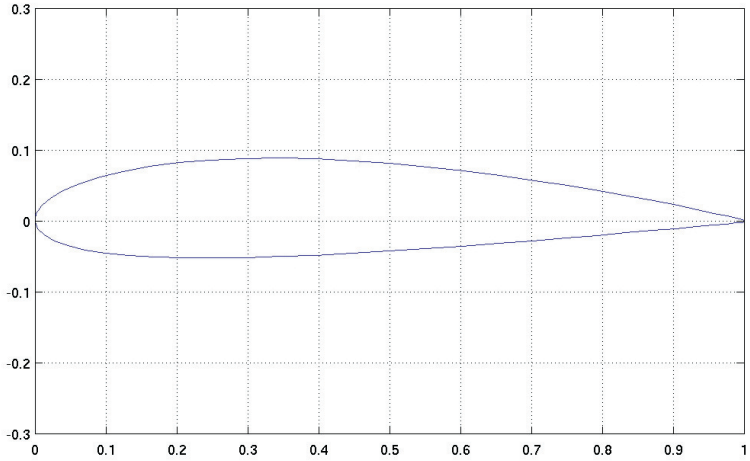

Figure 4.1.4: *Airfoil section NACA 2414*

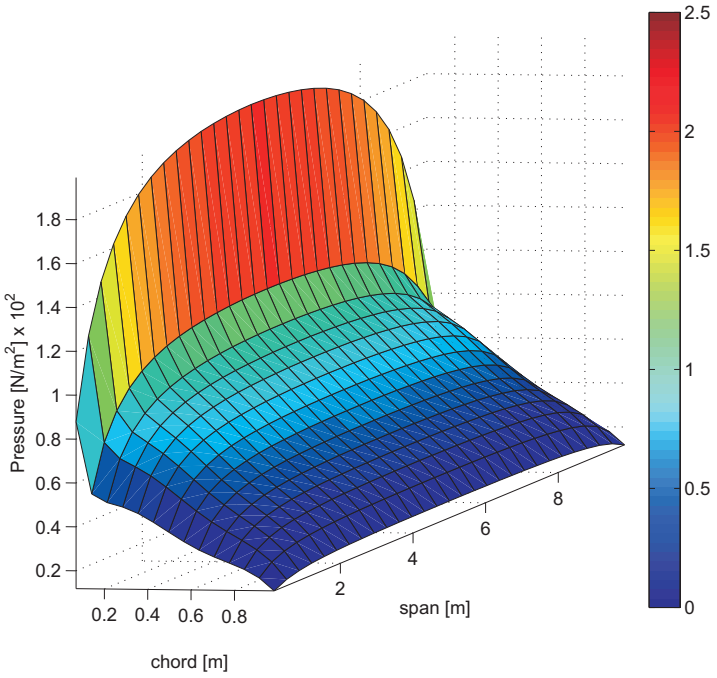

Figure 4.1.5: *Pressure distribution, asymmetric wing*

4.2 Wind turbine blade

For the case of a single wind turbine blade rotating around a horizontal axis in uniform flow the pressure distribution on the blade looks very different, as can be seen in figure 4.2.1. Here one full scale blade from the NREL 5MW wind turbine was used for the calculation.

Although the values at the leading edge are higher than at the trailing edge, as for a wing, it can be seen clearly that the difference in pressure is higher the closer the control point is to the tip of the blade. This can easily be explained with higher rotational speeds at the tip of the blade. Higher rotational velocities mean higher total relative velocities and therefore a higher dynamic pressure.

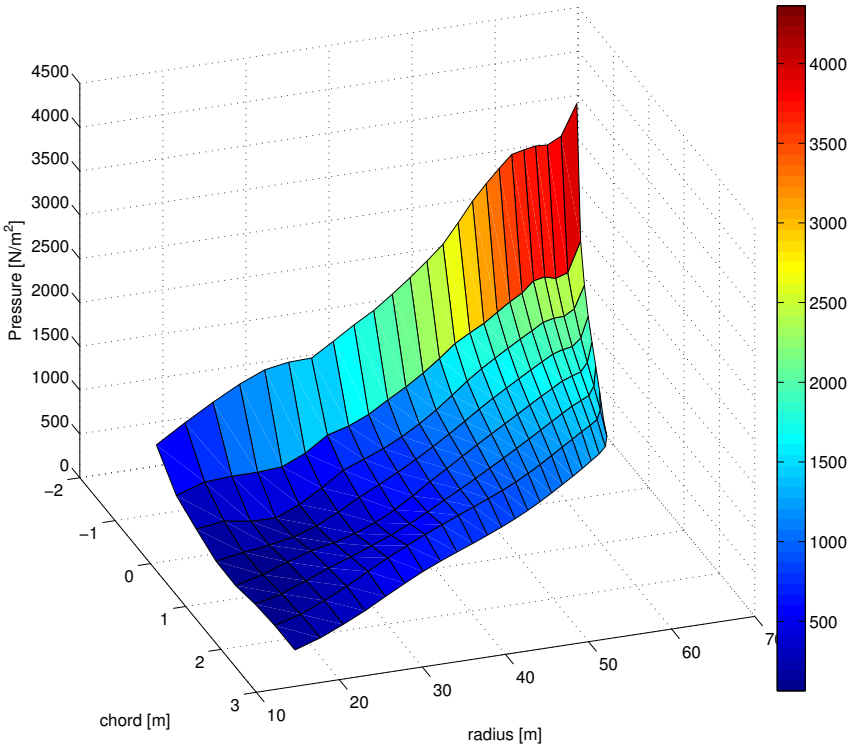

Figure 4.2.1: *Pressure distribution, single rotating turbine blade*

The same matter is reflected in figure 4.2.2 where the distribution of the normal force along the span with respect to the rotor plane is plotted. This is the force that causes the blade to bend in the direction of the wind. The normal force increases from zero first quickly, then linearly till it hits the maximum at approximately 90% of the total blade length. From there it drops quickly till zero at the tip.

The tangential force on the blade, see figure 4.2.3, which is responsible for the momentum on the power generator, in contrary, is nearly equally distributed. Close to the root and the tip the tangential force drops to zero. It has a maximum at approximately 65% of the total blade length. The reason for that nearly equal distribution is that the twist of the blade decreases from 13.3 degrees at the root to zero degrees at the tip. Therefore the tangential force does not increase closer to the tip although the total relative velocity does.

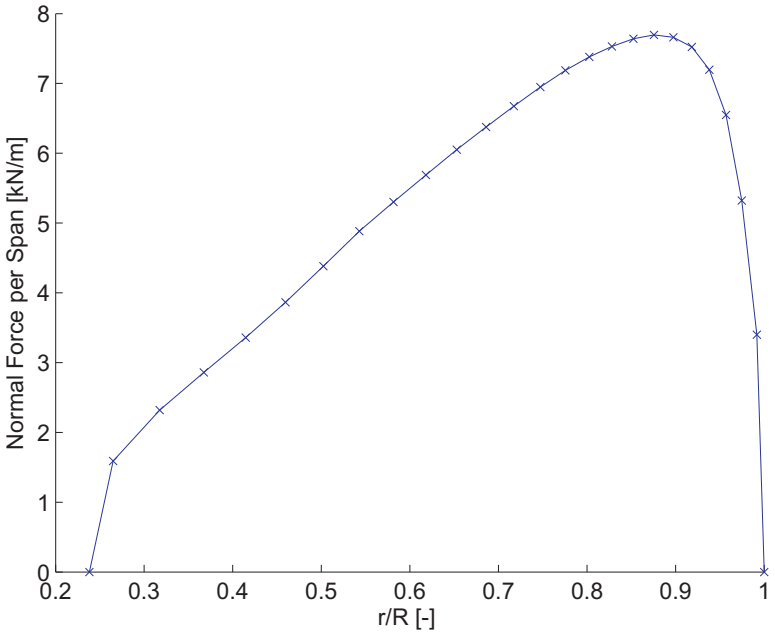

Figure 4.2.2: *Distribution of normal force along the span with respect to rotor plane, single rotating turbine blade*

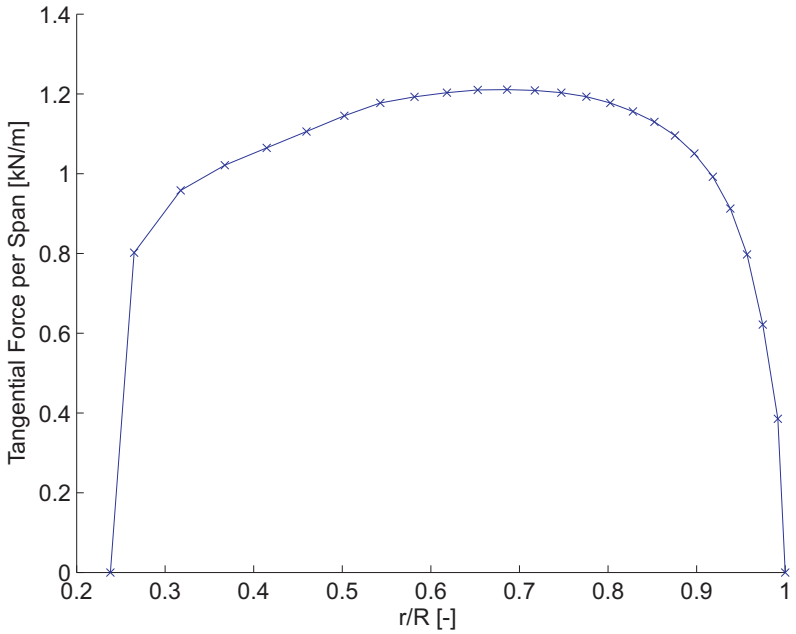

Figure 4.2.3: *Distribution of tangential force along the span with respect to rotor plane, single rotating turbine blade*

4.3 Wind turbine NREL 5MW

4.3.1 Grid analysis

In order to be able to run many different cases for different methods it is mandatory to find a grid size that is as fine as necessary but also as coarse as possible. Therefore the grid size of the panels on the blade (i, j) and the wake (k, j) as well as the wake length have been investigated. For the analysis a basic set of parameters was chosen, see table. 4.3.1. For each investigation all parameters are according to the table except for the investigated one. That parameter was varied from its maximum or a very high value till the smallest possible value.

To capture the difference that is caused by the change of the parameter a power ratio was chosen. This ratio consists of the calculated power outcome for the specific set of parameters divided by the power outcome of the investigated parameter at the highest value. Regarding the grid counter along the camber

Table 4.3.1: Basic set of parameters for grid analysis

Symbol	Description	Value
i	grid counter along camber line	5
j	grid counter from root to tip	9
k	grid counter from trailing edge till end of wake	18
w	wake length in rotations	1
q_∞	free stream velocity in meters per second	8
ω	rotational velocity in rad per second	1.0032

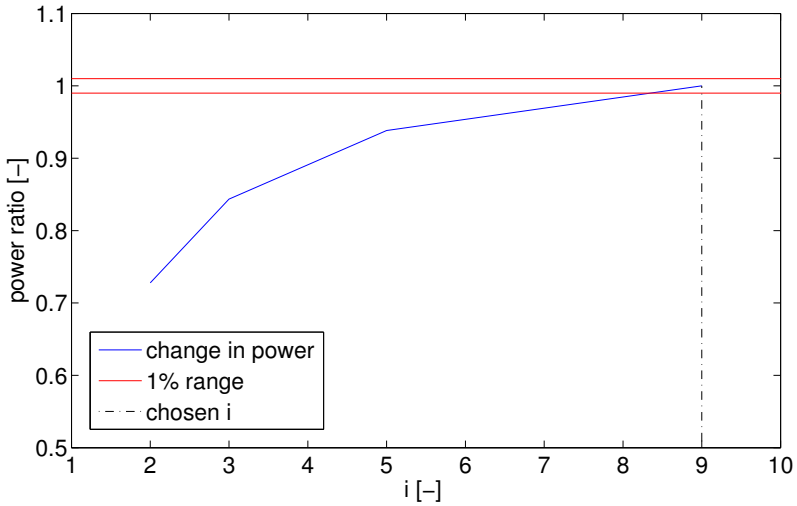

Figure 4.3.1: *Change of power due to a change of the grid size in chordwise direction*

line, i, it can be seen in fig 4.3.1 that the power ratio drops quickly when i becomes coarser. The red lines stand for the 1% range of the power ratio for the highest value of i. To stay in between the two lines i equals nine has to be chosen. In figure 4.3.2 the grid number from root to tip was investigated. Here

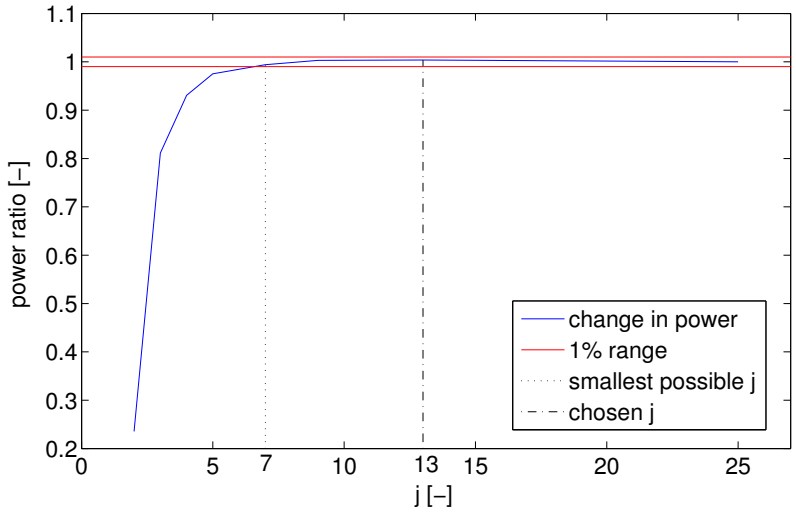

Figure 4.3.2: *Change of power due to a change of the grid size in radial direction*

it can be seen that while decreasing j the power ratio stays in the 1% range till j equals seven and drops quickly afterwards. Hence due to graphical problems (recall: tangential and normal forces are plotted along the turbine blade from root to tip) j equals 13 was chosen for further investigations.

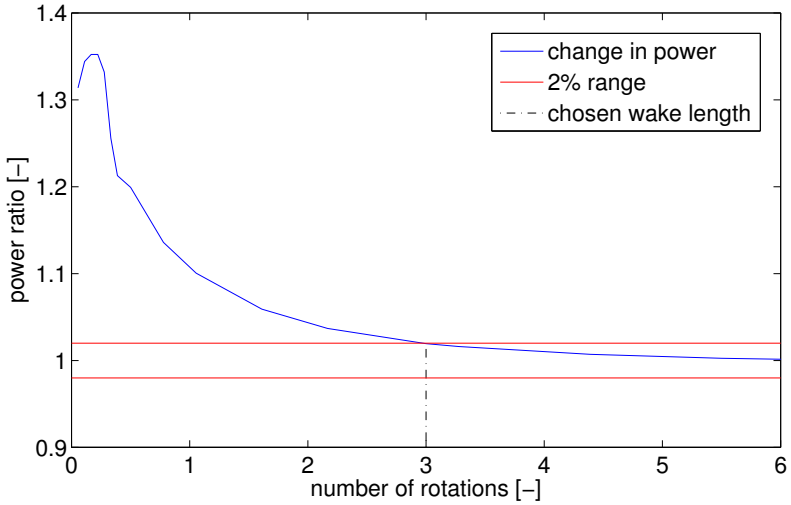

Figure 4.3.3: *Change of power due to a change of wake length behind the wind turbine*

Figure 4.3.3 shows the change in power ratio due to a change in the wake length behind the wind turbine. It can be seen that the power ratio first increases slightly before it drops exponentially. After five rotations the curve starts to flatten out. For the parameter study wake length was varied between 0.03 and 6 revolutions. In that case three revolutions are still within the 2% range, which is acceptable considering how much computational time is saved by decreasing the number of revolutions.

Since the number of grid nodes from the trailing edge till the end of the wake is no absolute value (for a change of the wake length the wake panel size changes), the angle β is introduced. This is the angle between two wake grid points in the wake. For a wake length of 360 degrees and 19 wake grid nodes there are 18 panels, which means β equals to 20 degrees. In figure 4.3.4 β is varied from 10 to 120 degrees. The power ratio here decreases linearly till 90 degrees and drops after that. The biggest possible β and therefore the smallest k within the 1% range is 20 degrees.

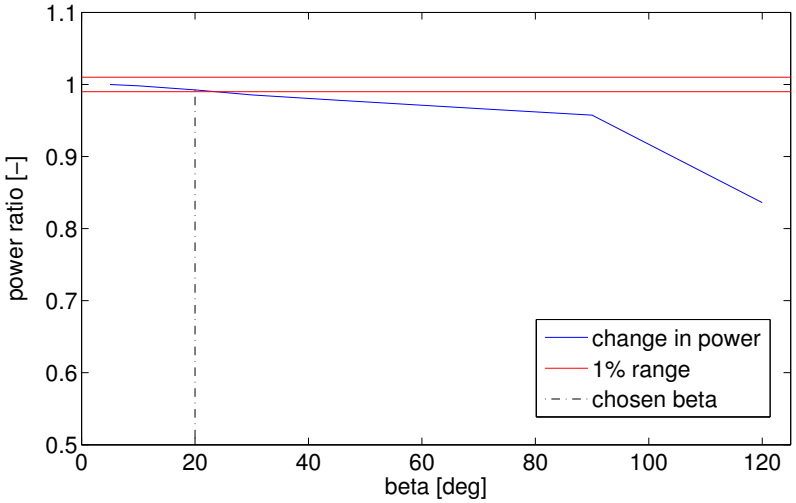

Figure 4.3.4: *Change of power due to a change of the grid size of the wake*

In conclusion the following parameters were chosen for all further investigation.(Table 4.3.2)

Table 4.3.2: Chosen parameters for further investigation

Symbol	Description	Value
i	grid counter along camber line	9
j	grid counter from root to tip	13
β	angle between two wake grid points in the wake in degrees	20
w	wake length in rotations	3

4.3.2 Comparison of Vortex Panel Method (VPM), Reduced Vortex Panel Method (RVPM) and Lifting Surface Method

In this section the vortex panel method (VPM) with a number of panels chordwise, the reduced vortex panel method (RVPM) with one panel chordwise and the lifting surface method are compared to each other. The induced velocity, the effective angle of attack, the strength of vorticity γ, the normal and the tangential force distribution are evaluated. Additionally two different wake shapes are used for the computation, the prescribed helical wake and the updated helical wake.

Figure 4.3.5 shows the induced velocities along the blade from root to tip. For the reduced vortex panel method and the lifting surface method the induced velocities are the ones located at the control points since there is only one control point in chordwise direction. In the lifting surface method the wake consist of the trailing vortices and the vortex panel methods use vortex rings to model the wake. Nevertheless, in steady-state condition the wake in VPM and RVPM is similar to trailing vortices.

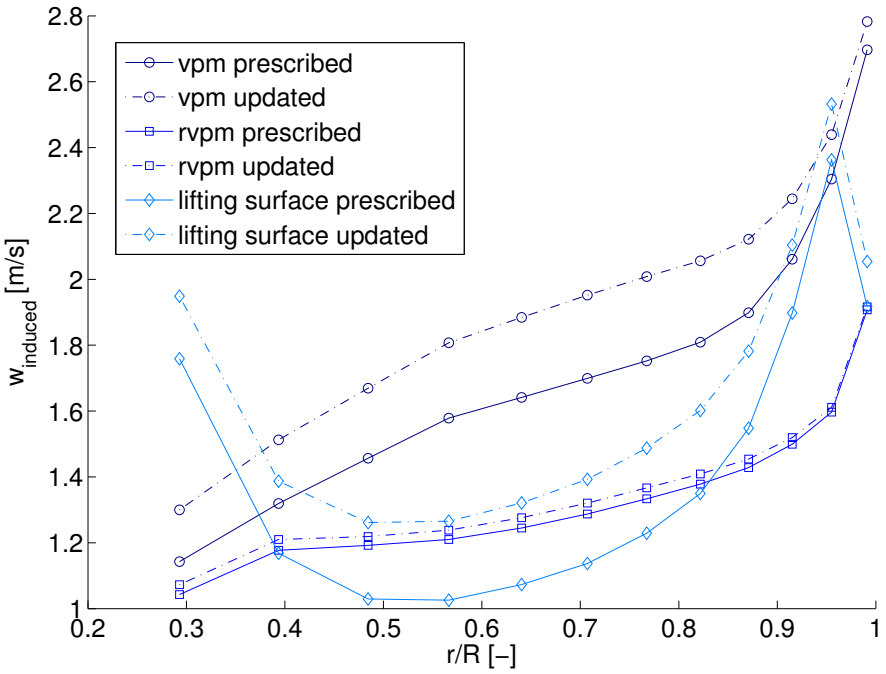

Figure 4.3.5: *Induced velocity distribution normal to rotor plane*

The induced velocities of the vortex panel method are the average values of all control points in one airfoil section. For the all vortex panel lines the induced velocity increases from a value around 1.2 $\frac{m}{s}$ to 2.8 $\frac{m}{s}$ (VPM) and 1.9 $\frac{m}{s}$ (RVPM). The values of the lifting surface method in contrary decrease from between 1.9 and 2.0 $\frac{m}{s}$ to an minimum at 50% of the total blade length and increase again approaching the values of the vortex panel method close to the tip. However, the

last data point at 98% of the total blade length resembles the reduced vortex panel method. Moreover, it is obvious that the values of the updated wake are consistently higher than the ones of the prescribed wake. Due to updating where the wake includes the induced velocity, the wake is overall closer to the wind turbine than for the prescribed wake. Therefore the impact on the blade in the form of induced velocity is higher.

Since the induced velocity has a big impact on the angle of attack, the effective angle of attack changed correspondingly. The red line in figure 4.3.6 is the geometric angle off attack that is calculated from free stream and rotational velocity. All lines with markers are effective angles of attack, that include the effect of the induced velocity. As expected, those angles are much smaller than the geometric angle of attack, especially where the induced velocity is high. Here, the values of the updated wake are consistently lower than the ones of the prescribed wake. The distributions of the strength of vorticity γ in figure 4.3.7 are very

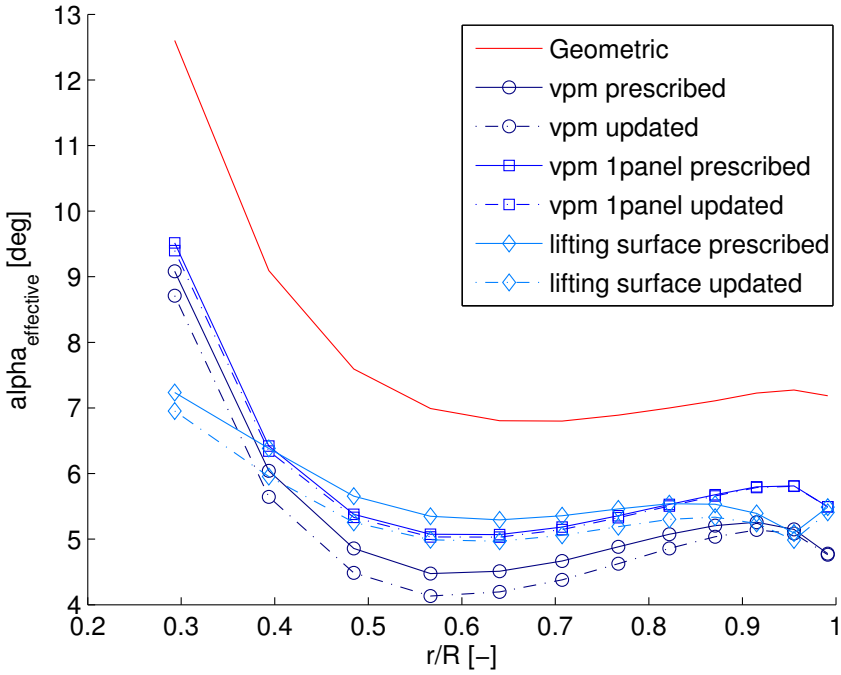

Figure 4.3.6: *Effective angle of attack along the blade*

similar at the tip of the turbine blade but the further to the root the more they differ. From tip to root the values increase very quickly to values around 40 $\frac{m^2}{s}$ at approximately 85% of the total blade length and decrease then to values between 30 and 40 $\frac{m^2}{s}$. Here, the values of the updated wake are consistently lower than the ones of the prescribed wake.

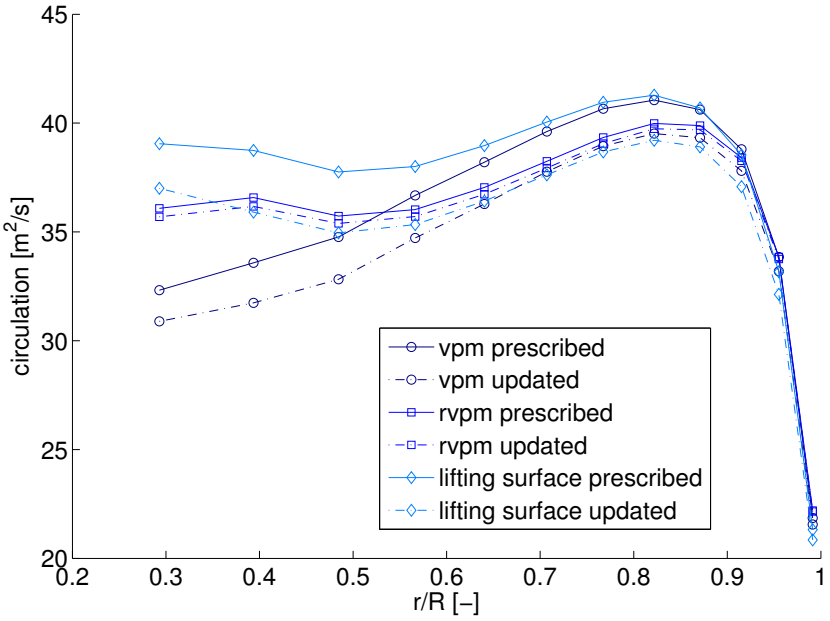

Figure 4.3.7: *Vortex distribution along the blade*

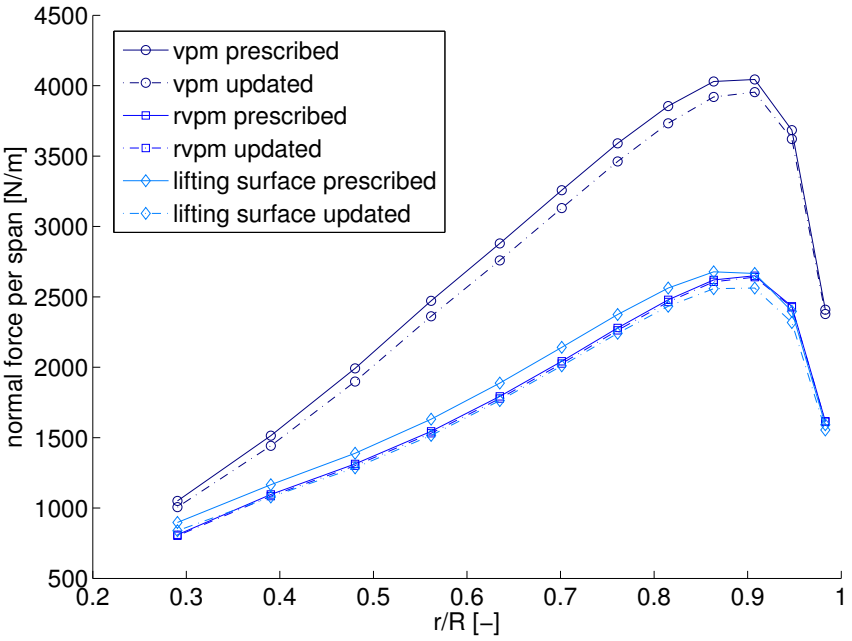

Figure 4.3.8: *Normal velocity distribution along the blade*

The results of the normal, figure 4.3.8, and tangential force, figure 4.3.9, are similar to the results for a single turbine blade. The difference is the magnitude

of the values. It is smaller than for one turbine blade because those plots were generated for higher wind speeds and there are now three blades in the same area instead of one. Particularly conspicuous is that the values of the reduced vortex panel method and lifting surface method are about 40% lower than the values of the vortex panel method. That can be explained through the disregard of the camber line curvature.

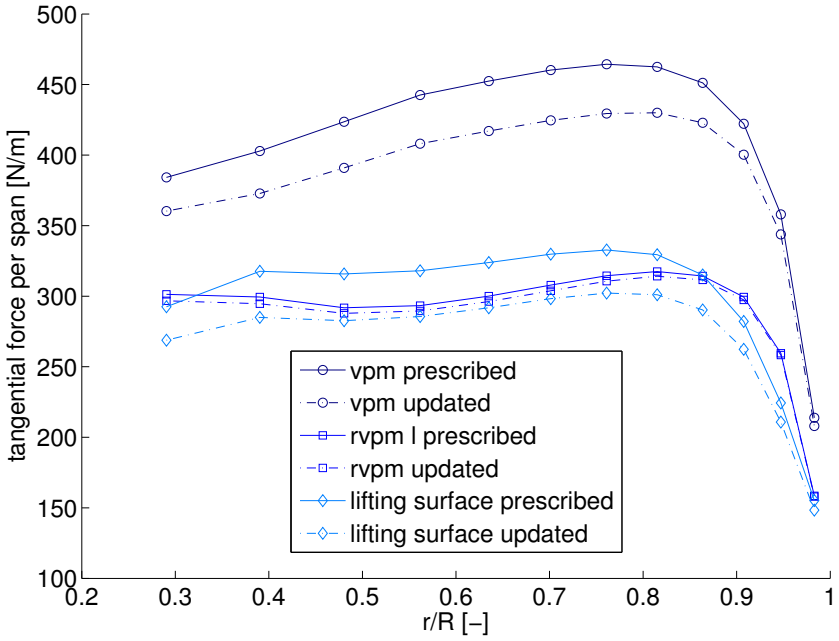

Figure 4.3.9: *Tangential velocity distribution along the blade*

4.3.3 Wake shapes

In this section the wake behind the wind turbine is plotted for one turbine blade only in order to increase clarity. The rotor plane is in the $x-y$-plane and the turbine rotates clockwise, seen in positive z-direction. The free stream velocity is in positive z-direction. Here three rotations of the turbine blade are plotted. In figure 4.3.10 the prescribed helical wake is shown. It is a simple wake calculated according to equation 3.3.1 with a total wake length of 170 m for three rotations. For the updated wakes the wake shape was found in an iterative process till the residual was smaller than 0.01. In these cases it required only three iterations. As expected, the updated wake shapes are compressed compared to the prescribed wake due to the addition of the the induced velocities (see figures 4.3.11, 4.3.12 and 4.3.13). The total wake length of the wake of the vortex panel method, the reduced vortex panel method and the lifting surface method is between 126 and 130 m. The main difference between the three updated wakes is their shape along the radius. All shapes are according to their induced velocity distribution in figure 4.3.5.

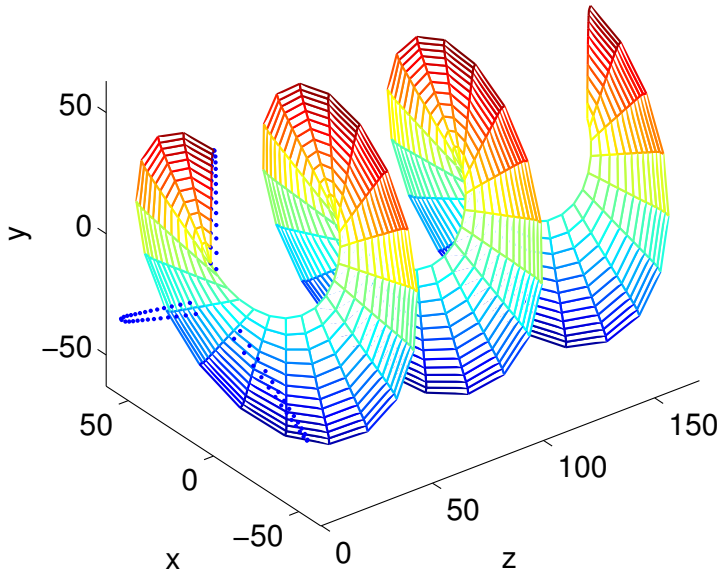

Figure 4.3.10: *Prescribed helical wake shape*

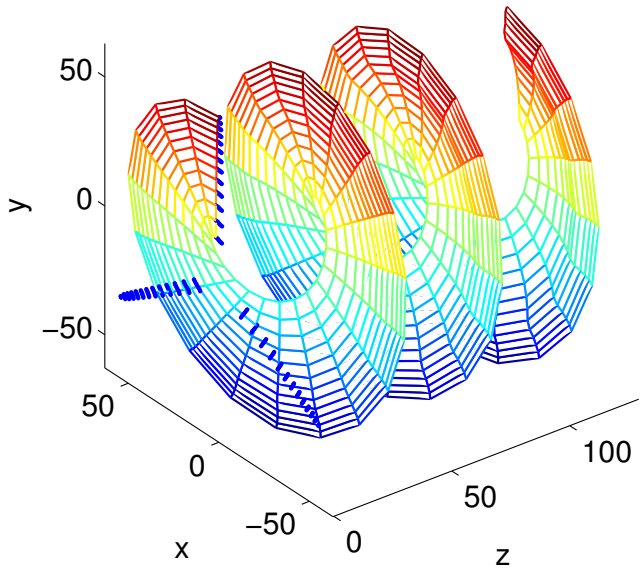

Figure 4.3.11: *Updated wake shape after 3 iterations with vortex panel method*

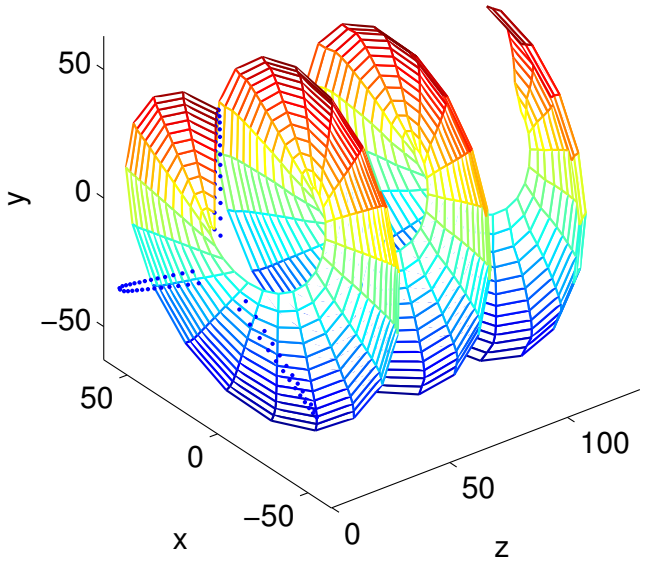

Figure 4.3.12: *Updated wake shape after 3 iterations with reduced vortex panel method*

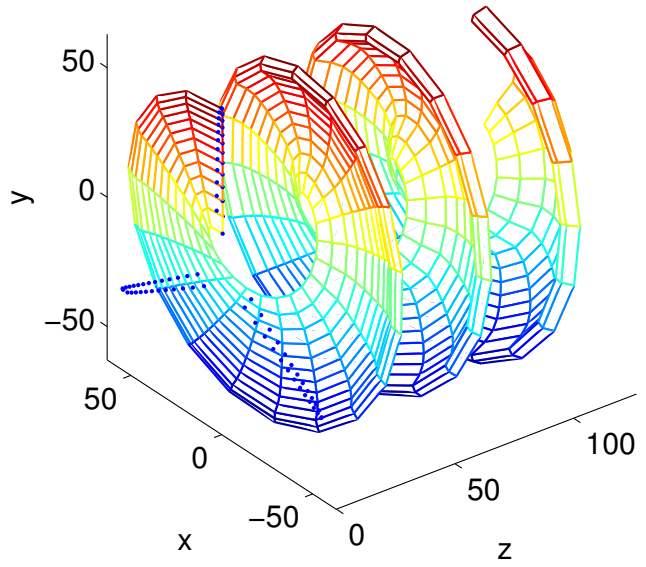

Figure 4.3.13: *Updated wake shape after 3 iterations with lifting surface method*

4.4 Validation

To validate the results data from three different sources was investigated. Since there was only data available for certain cases with different wind speeds and rotational velocities, the validation section was split up in GENUVP and BEM & CFD. GENUVP is an unsteady flow solver based on vortex blob approximations developed for rotor systems by National Technical University of Athens (courtesy of Prof. Spyros Voutsinas) [11]. GENUVP includes a dynamic stall model as well as friction which is considered based on the C_d vs. α table [10]. In this section the vortex panel methods with updated wake were used for all figures.

4.4.1 GENUVP

For the comparison with GENUVP the free stream velocity was 8 $\frac{m}{s}$ and the rotational velocity 9.6 rpm. When comparing the induced velocities to GENUVP in figure 4.4.1 it can clearly be seen that the vortex panel method resembles the GENUVP data best in terms of magnitude but the lifting surface method is better in terms of shape. Both, GENUVP and lifting surface, have a maximum at the root and close to the tip. The vortex panel methods have only one at the tip.

The same relation can be seen in figure 4.4.2 where the effective angle of attack is plotted. The red line still shows the geometric angle of attack excluding induced velocities. Again the vortex panel method resembles the GENUVP magnitude but the lifting surface method the shape. Nevertheless the results for normal (figure 4.4.3) and tangential force (figure 4.4.4) show that the vortex panel method is much closer to the GENUVP data. Indeed the normal force is nearly the same.

The fact that physical phenomena like friction and dynamic stall were not addressed explains why the tangential force is too high compared with GENUVP which does include engineering models for stall and friction.

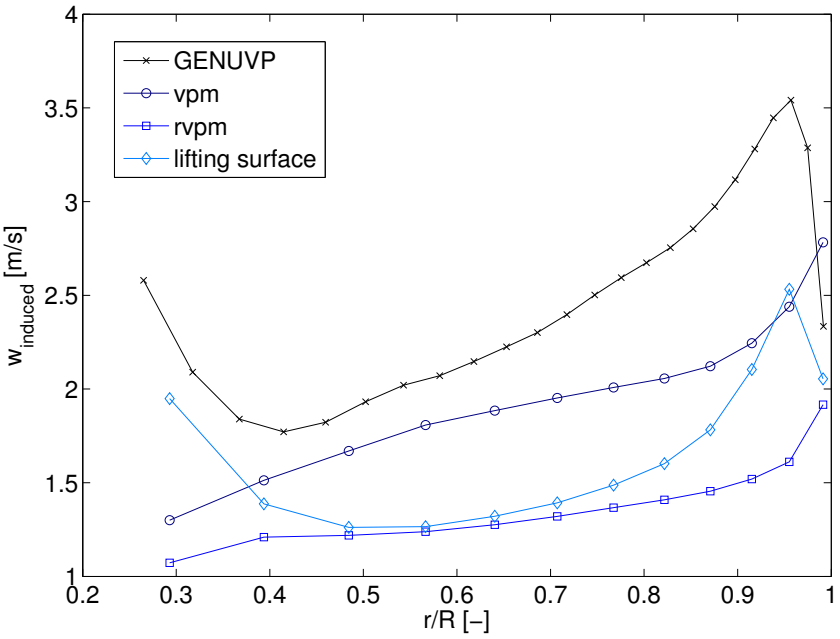

Figure 4.4.1: *Induced velocity distribution normal to rotor plane*

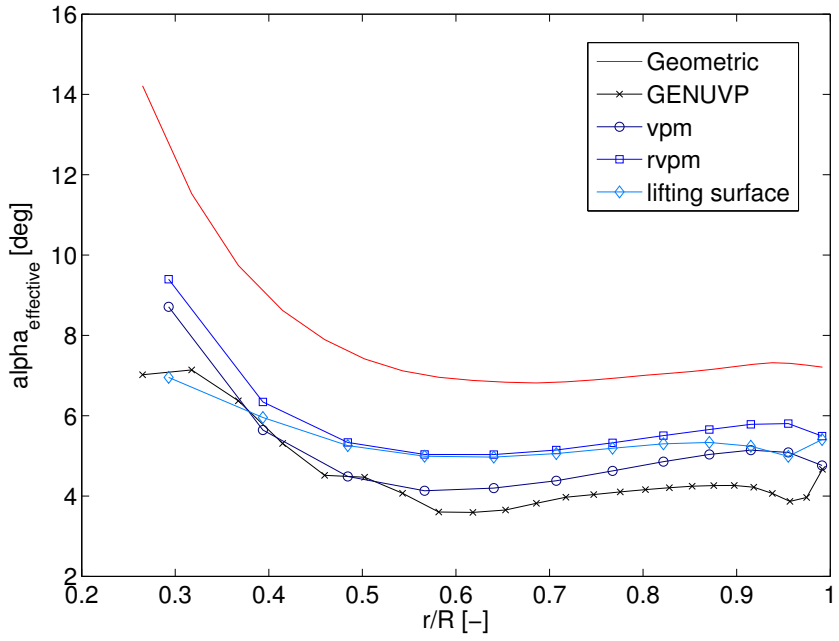

Figure 4.4.2: *Effective angle of attack along the blade*

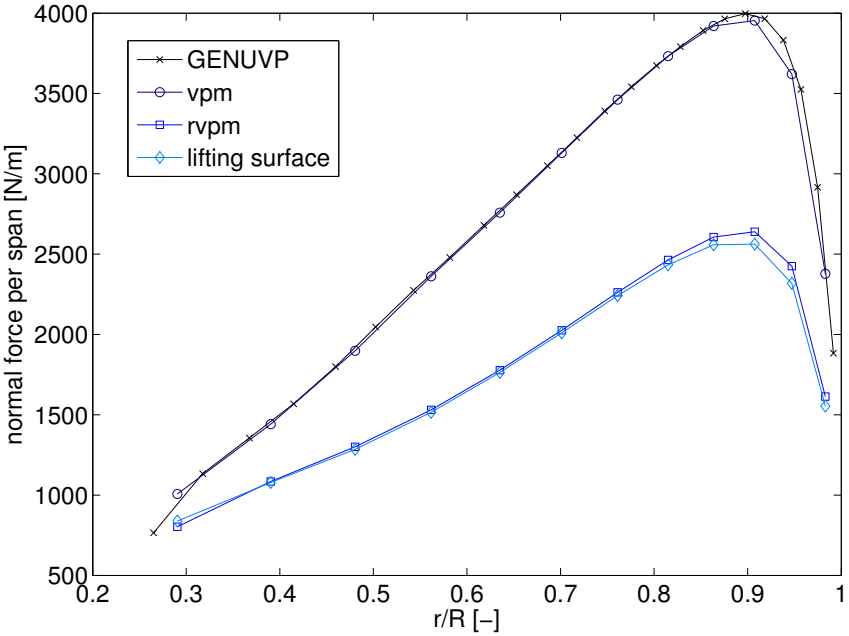

Figure 4.4.3: *Normal force distribution along the blade*

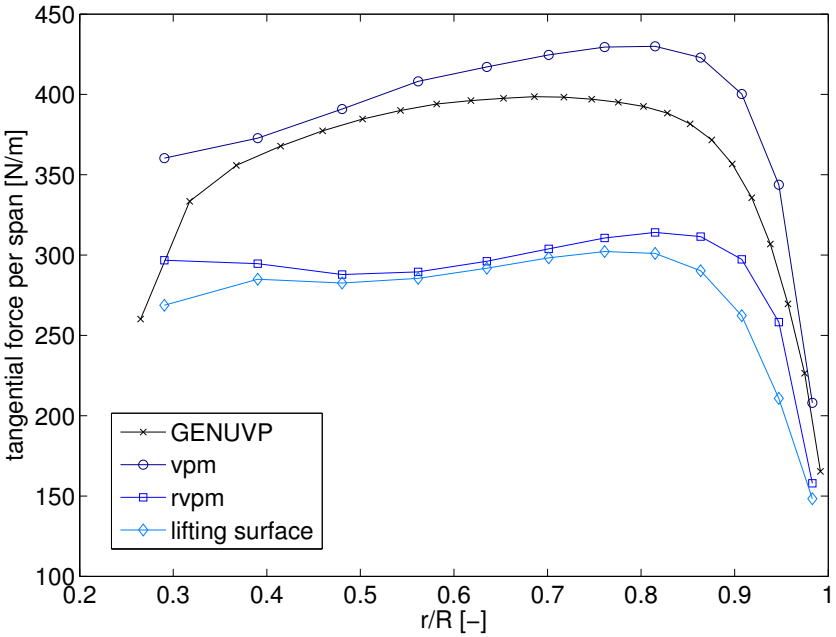

Figure 4.4.4: *Tangential force distribution along the blade*

4.4.2 CFD & BEM

For every flow model it is important to compare the results with CFD if experimental data is not available since CFD is considered to be most accurate. Furthermore the results are compared to BEM data, because BEM is very fast and suitable for wind turbine analysis. Therefore it is a good reference for vortex methods. Here the free stream velocity is 11.4 $\frac{m}{s}$ and the rotational velocity is 12.1 rpm.

Again the vortex panel method gives very good results for the normal force distribution (figure 4.4.5), even better than BEM. But when it comes to tangential forces (figure 4.4.6) the vortex panel method can not compete with BEM. Surprisingly even the reduced vortex panel method is closer to the CFD data than VPM. However, as mentioned in section 4.4.1 "GENUVP", all vortex panel methods neglect the influence of dynamic stall and friction. Therefore the results should be lower when including those. Then the results of the vortex panel method should be closer to the CFD data.

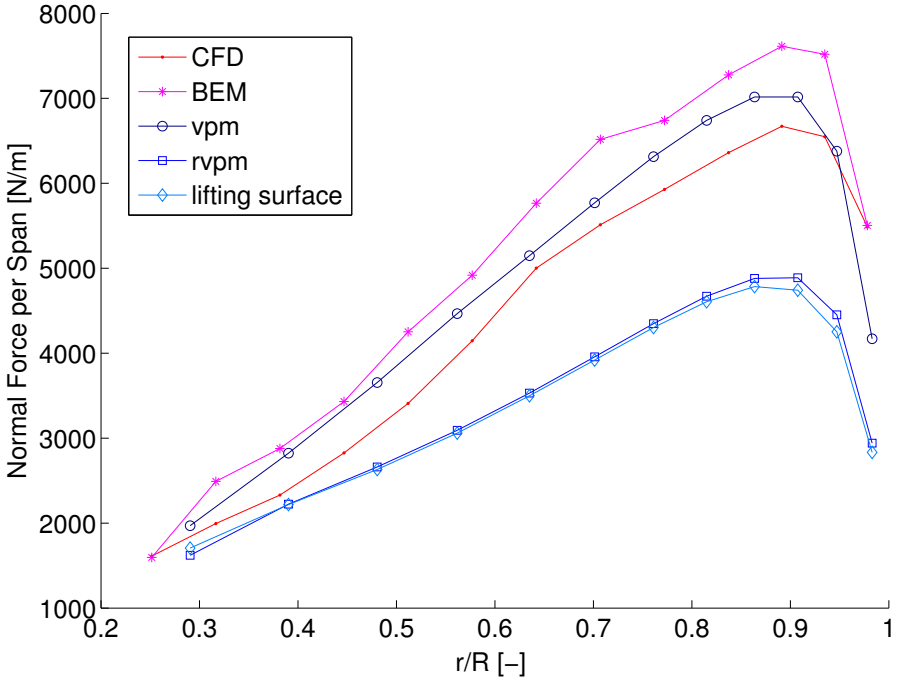

Figure 4.4.5: *Normal force distribution along the blade*

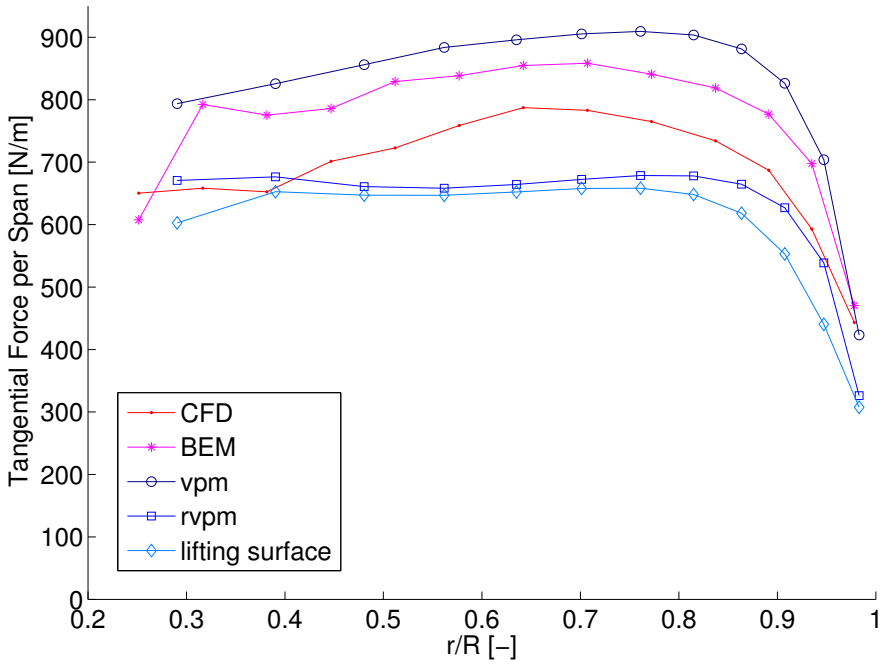

Figure 4.4.6: *Tangential force distribution along the blade*

5 Conclusion

In conclusion can be said, that the vortex panel method is very suitable for wind turbine analysis. Although engineering models for stall and friction were not included in the calculation the results of a basic vortex panel method are similar to CFD and GENUVP data. In particular the normal force with respect to the rotor plane is captured by the vortex panel method accurately.

Simpler vortex methods as the reduced vortex panel method and the lifting surface method are much faster that the vortex panel method, but they should not be used to model wind turbine blades. Since they neglect the curvature of the camber line they are not able to produce accurate enough results.

Therefore choosing the right grid is very important for vortex panel methods. Especially along the camber line there should not be any simplifications, which means the grid should be very fine.

5.1 Future work

In order to prove the advantages of vortex panel methods compared to BEM it is important to test it for unsteady conditions such as changing wind speeds and non-uniform flows. Therefore the free vortex concept must be applied to such flows.

Furthermore the root of the blade, the hub and the tower of the wind turbine should be included in the model so that the influence of the whole wind turbine is taken into account. However the vortex panel method itself can be improved as well. Engineering models like dynamic stall models, dynamic inflow, friction or wind turbulence can be included in the code.

A Appendices

A.1 Methods to simulate flow fields

A.1.1 BEM

Blade Element Momentum Theory combines two methods that analyze the aerodynamics of wind turbines. The first method is to use a momentum balance on a rotating stream tube in which a turbine is placed. The second one is to examine the forces generated by the airfoil lift and drag coefficients at various sections along the blade. These two methods then give a series of equations that can be solved iteratively. [6] For more information see also [1].

A.1.2 CFD

Computational Fluid Dynamics (CFD) uses numerical methods and algorithms to solve and analyze problems that concern fluid flows. That involves the solution of the Navier-Stokes equation in fluid dynamics.

A.2 Airfoil geometries

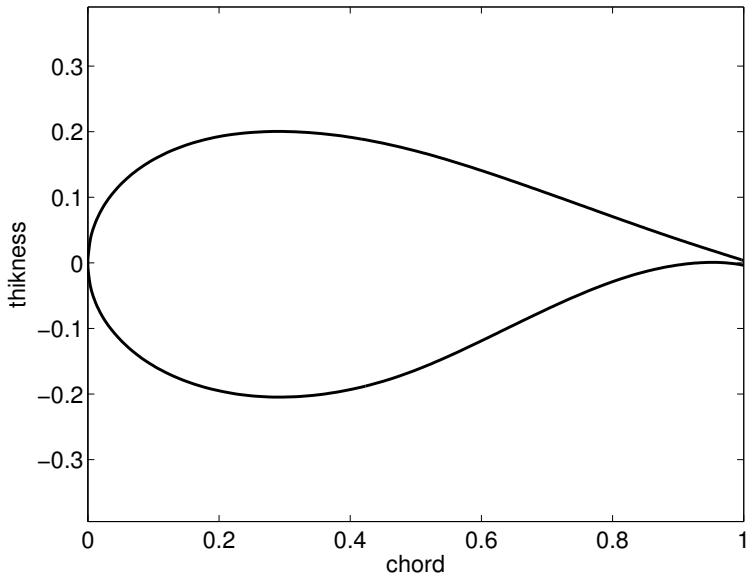

Figure A.2.1: *Airfoil geometry DU40_A17*

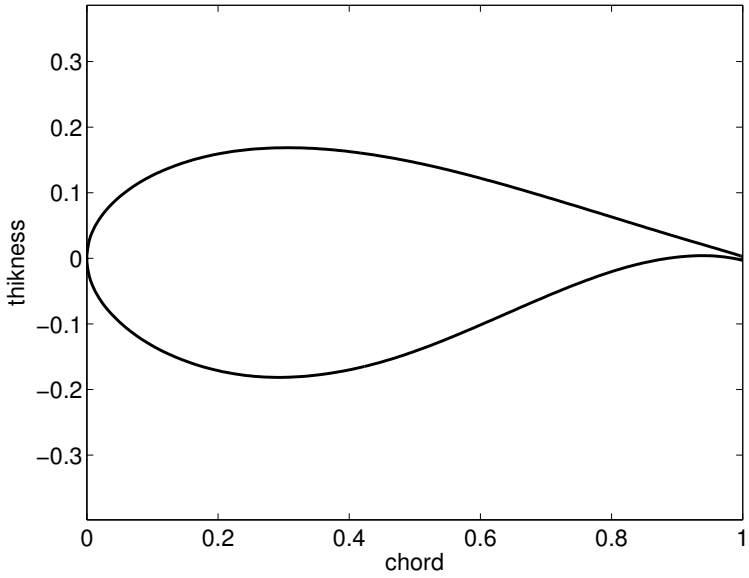

Figure A.2.2: *Airfoil geometry DU35_A17*

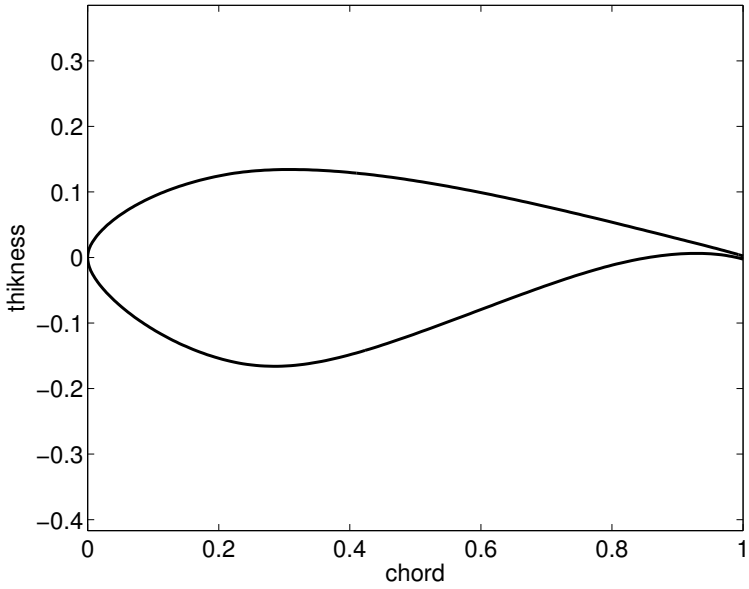

Figure A.2.3: *Airfoil geometry DU30_A17*

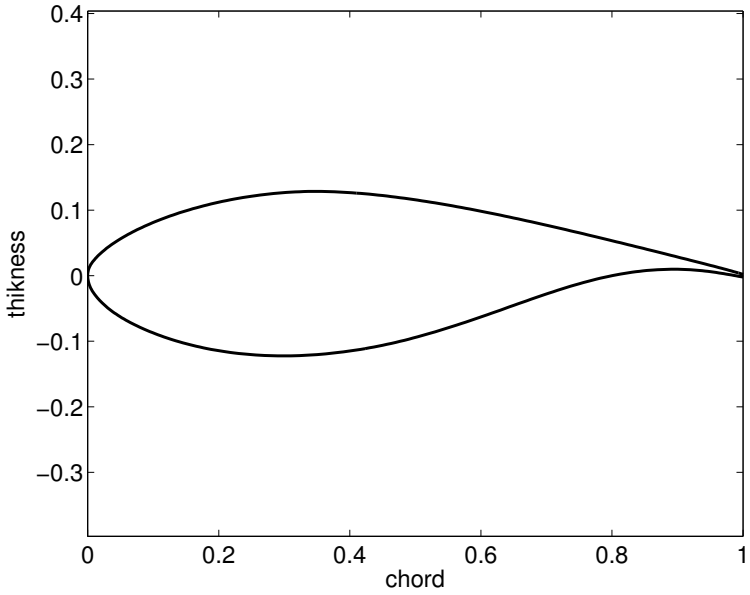

Figure A.2.4: *Airfoil geometry DU25_A17*

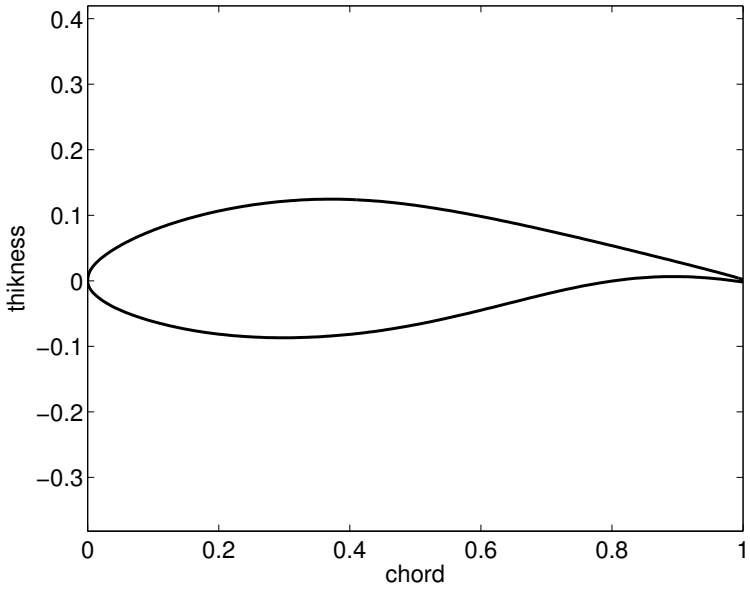

Figure A.2.5: *Airfoil geometry DU21_A17*

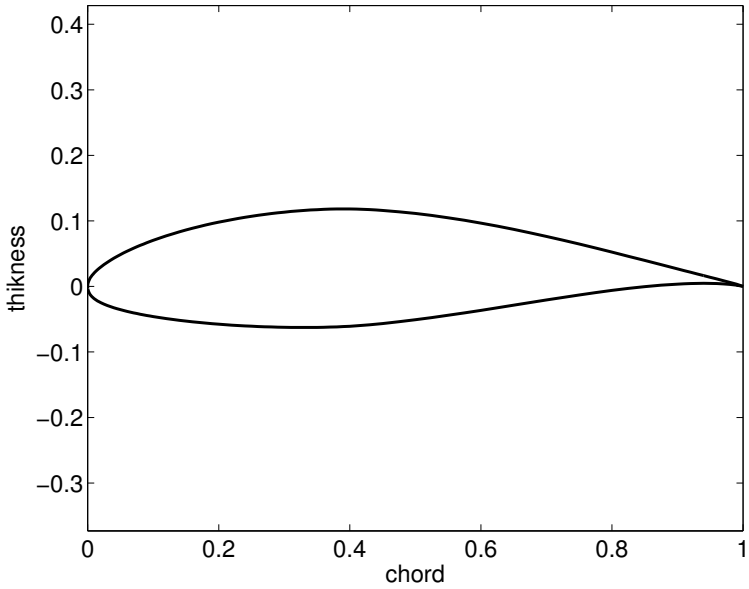

Figure A.2.6: *Airfoil geometry NACA64_618*

References

[1] H. Abedi. "Aerodynamic Loads on Rotor Blades". MA thesis. Chalmers University of Technology, 2011. ISBN: 1652-8557.

[2] J. D. Anderson. *Fundamentals of Aerodynamics*. McGraw-Hill Science/Engineering/Math, 2001. ISBN: 0072373350.

[3] K. R. Dixon. "The Near Wake Structure of a Vertical Axis Wind Turbine". MA thesis. Delft University of Technology, 2008.

[4] G. A. Flandro, H. M. McMahon, and R. L. Roach. *Basic Aerodynamics: Incompressible Flow*. Cambridge University Press, 2011. ISBN: 978-05-218-0582-7.

[5] R. W. Fox, P. J. Pritchard, and A. T. McDonald. *Introduction to Fluid Mechanics*. 7th. John Wiley & Sons, Inc., UK, 2010. ISBN: 978-81-265-2317-7.

[6] G. Ingram. *Wind Turbine Blade Analysis using the Blade Element Momentum Method*. Durban University. 2011. URL: `http://www.dur.ac.uk/g.l.ingram/download/wind_turbine_design.pdf`.

[7] T. R. Jackson. "The Geometric Design of Functional Shapes". MA thesis. Princeton University, 1997.

[8] J. Jonkman et al. *Definition of a 5-MW Reference Wind Turbine for Offshore System Development*. National Renewable Energy Laboratory, 2009.

[9] J. Katz and A. Plotkin. *Low-Speed Aerodynamics*. Cambridge University Press, 2001. ISBN: 0-521-66219-2.

[10] D. G. Opoku et al. "ROTORCRAFT AERODYNAMIC AND AEROACOUSTIC MODELLING USING VORTEX PARTICLE METHODS". In: *ICAS 2002-2.1.3*. 23rd Congress of International Council of the Aeronautical Sciences, Toronto, Canada, 2002.

[11] V. A. Riziotis, S. G. Voutsinas, and A. Zervos. *INVESTIGATION OF THE YAW INDUCED STALL AND ITS IMPACT TO THE DESIGN OF WIND TURBINES*. National Technical University of Athens. 1996. URL: `http://www.fluid.mech.ntua.gr/wind/vasilis/vasiewec.html`.

[12] M. Roura et al. "A panel method free-wake code for aeroelastic rotor predictions". In: *Wind Energy* 13 (2010), pp. 357–371.

[13] UIUC Applied Aerodynamics Group. *UIUC Airfoil Coordinates Database*. 2012. URL: `http://www.ae.illinois.edu/m-selig/ads/coord_database.html`.

[14] L. J. Vermeer, J. N. Sørensen, and A. Crespo. "Wind turbine wake aerodynamics". In: *Progress in Aerospace Sciences* 39 (2003), 467–510.

[15] S. G. Voutsinas. "Vortex methods in aeronautics: how to make things work". In: *International Journal of Computational Fluid Dynamics* 20 (1 2006).